UTRECHT UNIVERSITY

MASTER THESIS

Towards source estimation: Modeling total Methane columns in Europe

Author:
Joanne HULLEGIE

Supervisors:
Prof. Dr. Maarten Krol (IMAU)
Dr. Ir. Arjo Segers (TNO)
Dr. Ir. Hugo Denier van der Gon (TNO)

August 24, 2018

A thesis submitted in fulfillment of the requirements
for the degree of Master of Science

in the

Atmospheric Physics and Chemistry Group (APCG)
Institute for Marine and Atmospheric Research (IMAU)

TNO

UTRECHT UNIVERSITY

Abstract

Faculty of Science
Institute for Marine and Atmospheric Research (IMAU)

Master of Science

Towards source estimation: Modeling total Methane columns in Europe

by Joanne HULLEGIE

Methane gas is the second-largest contributor to the greenhouse effect. Under the 2015 Paris Agreement, worldwide methane emissions are to be reduced. To monitor these reductions it is important to be able to identify sources of methane. Bottom-up emission inventories estimate methane sources from activities and emission factors. By implementing these emissions in a Chemical Transport Model (CTM), methane concentration can be predicted and compared with observations. The aim of this study is to work towards the use of LOTOS-EUROS (CTM) and TROPOMI satellite measurements to verify European emission inventories. Study objectives are getting insight in methane emission inventories and evaluating the model sensitivity and performance. The latter will be achieved by comparing the model simulations with methane observations. Additionally, we will take a first look at the TROPOMI data and discus some retrieval difficulties.

This study finds that LOTOS-EUROS is able to simulate the methane volume mixing ratios in the right order magnitude. However, there seems to be an incorrect VMR gradient simulated in the stratosphere.

Preliminary results from TROPOMI suggest that strong source regions can be quantified. Besides, they indicate that LOTOS-EUROS simulates locally smaller enhancements than TROPOMI measures. More TROPOMI data is needed to be conclusive on this.

Preface and Acknowledgements

This document presents the master thesis "Towards source estimation: Modeling total Methane column in Europe". This thesis is written to fulfill the graduation requirements of the master program Climate Physics at Utrecht University. This project was supervised by Prof. Dr. Maarten Krol from Utrecht University, who I would like to thank for the guidance given during my thesis.

The project was carried out at TNO, the Netherlands Organisation for applied scientific research and I would like to express my gratitude to my daily supervisors, Dr. Ir. Arjo Segers and Dr. Ir. Hugo Denier van der Gon. Thank you for all the guidance, help and talks we had during this project. I also wish to thank my other colleagues at TNO, who made me feel very welcome.

During this project I cooperated with people from different institutes. Therefore I wish to thank Prof. Dr. Ilse Aben (SRON, VU), Prof. Dr. Ir. Sander Houweling (SRON, VU) and Dr. Sudhanshu Pandey (SRON) for their feedback.

Contents

Chapter 1

Introduction

Methane (CH_4) is the second most abundant anthropogenic greenhouse gas in the atmosphere, after carbon dioxide (CO_2). Despite its low concentration relative to CO_2, it is still very potent since it has a stronger infrared radiation absorption per molecule. Methane contributes to 17% of the total radiative forcing of all greenhouse gases (Myhre et al., 2013). The global atmospheric CH_4 level was equal to 720 ppb in 1750 and has reached a level of 1800 ppb by 2011. This is more than double, and as such the increase in atmospheric methane concentration has become a topic of interest and has been studied widely (Blake et al., 1982; Neef, van Weele, and van Velthoven, 2010; Kirschke et al., 2013).

On December 21 of 2015 the Paris Agreement was signed by 195 countries to keep global warming below 2 degrees. Under this agreement, every country has to implement its own policies to reach this goal. Reducing methane emissions is often part of this policy. However, to identify areas with the potential to reduce emissions, quantification of the current methane emissions is required. There are several methods two quantify emissions. One is to simulate methane concentration with a chemical transport model. Comparing the simulated fields with measurements gives information about the emissions that were implemented in the model. When compared to instruments with large coverage and high resolution, it could provide information that will help to identify methane sources on a global scale.

The goal of this study is to simulate the methane volume mixing ratio (VMR) with a Chemical Transport Model (CTM), to evaluate its performance and to draw conclusions on the ability of satellite data to identify methane sources. The model performance will be evaluated by comparing model simulations with several measurement instruments: continuous in situ ground based observations, observations from the Greenhouse gases Observing SATellite (GOSAT) and observations from several stations from the Total Carbon Column Observing Network (TCCON). Observation of the recently launched TROPOMI instrument will provide information on the ability of satellites to identify methane sources.

To reach these goals an attempt is made to answer the following questions:

1. What are the known sources for methane and how are they quantified in inventories?
2. How sensitive are simulated model fields for different emission input and boundary conditions?
3. How does the model perform compared to methane observations?
4. Are the first TROPOMI data able to identify European emission hot spots?

This report consist of six Chapters: introduction, theoretical background, methods, results, discussion and conclusion of this study. In chapter 2 we will elaborate more on methane and the use of satellite data to estimate the volume mixing ratio. In chapter 3 the calculations of the total column and the comparison of the model with different measurements will be explained. In chapter 4 the model performance will be evaluated by discussing the comparison between the simulation and measurements. Additionally, the first results of TROPOMI will be studied. Improvements of the model will be proposed and recommendations for future studies will be made in chapter 5. Conclusions and a outlook will be presented in chapter 6.

Chapter 2

Methane modelling

2.1 Methane cycle

In this chapter background information will be given on atmospheric methane. The methane cycle will shortly be explained. Thereafter the main sources and sinks will be described. Additionally general information will be given on tools to study methane emissions.

2.1.1 Methane sources

Methane emission sources can be divided into four different categories:

- Thermogenic
- Pyrogenic
- Natural biogenic
- Man-made biogenic

In thermogenic sources methane is formed due to elevated temperature and pressure. Examples are geological sources which naturally emit fossil methane, such as seepages, mud volcanoes and geothermal vents. An example of non-natural emission of a geological source is the leakage from fossil fuel extraction and usage. Methane is emitted by pyrogenic sources as a result of incomplete burning of biomass and fossil fuels, for example peat fires (Saunois et al., 2016). Biogenic methane is formed through degradation of organic material in anaerobe conditions (Kirschke et al., 2013). This can be a natural source, for example emissions from wetlands, or anthropogenic source, for example emissions from rice paddies, ruminants livestock or landfills (Ciais et al., 2013).

Figure 2.1 shows the global methane budget estimate for the period 2003 to 2012. The above mentioned sources are divided in different categories making a distinction between natural and anthropogenic sources. Visible in this figure are the highest sources of methane: Fossil Fuel Use & Production ($\pm$ 20%), Agriculture & Waste ($\pm$ 33%) and Wetlands ($\pm$ 30%). The main sink of methane is the chemical degradation by OH radical together with soil uptake (Saunois et al., 2016).

In the next subsections these sources and sinks will be explained in more detail.

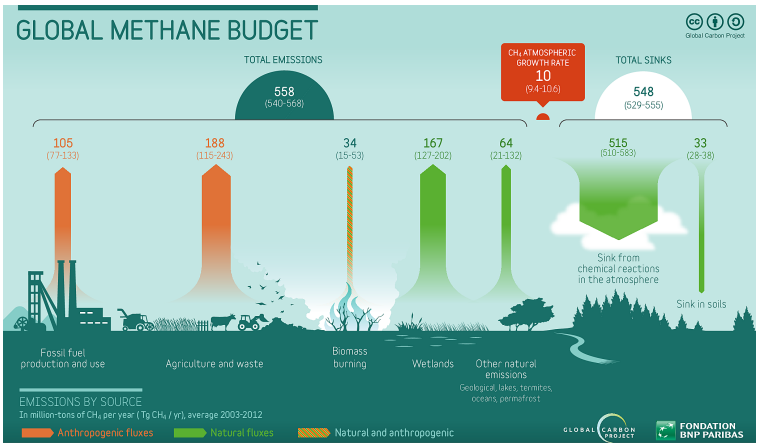

FIGURE 2.1: The Global Methane Budget 2000-2012 (Source: Saunois et al., 2016)

Fossil fuel use and production

Fossil fuel use and production are of geological and fossil origin but emitted due to human activity. For the time period 2003-2012 these emissions are estimated between 114–133 Tg CH_4 per year (Saunois et al., 2016). Usually these emissions come from transportation, exploitation and usage of oil (associated gas), coal (coal-bed gas) and natural gas (Saunois et al., 2016). These substances are used for the energy supply and therefore highly in demand. Natural gas is mainly composed of methane and small quantities (< 5%) of other hydrocarbons. It has been formed on a geological timescale when organic material (e.g. animals or plants) is buried under sediments. In time it is transformed due to heat and pressure into oil or gas (EIA, 2017). In the processes between extraction and usage, leakage can occur resulting in methane emissions.

Agriculture

The two largest emitters in agriculture are livestock and rice cultivation.

Livestock produces methane by anaerobic microbial activity in their digestive system. In the rumen of livestock metabolic hydrogen is produced (H) due to a constant flow of organic material (plants). Methanogenic archaea (a bacteria that lives in the rumen) converts hydrogen and carbon dioxide into methane which is thereafter mainly released through eructation (87%) (Saunois et al., 2016).

$$CO_2 + 4\,H_2 \longrightarrow CH_4 + 2\,H_2O \tag{2.1}$$

Rice is usually cultivated in flooded fields. Under these conditions organic matter is decomposed under anaerobic conditions again by methanogenic archaea. During this process methane is produced (methanogenesis) and released to the atmosphere (Saunois et al., 2016).

Waste

There are two sources which produce the majority of methane in the source category waste: (Non-)managed landfills (solid waste disposal on land) and waste water management. In landfills methanogenesis takes place. As organic waste is disposed on landfills, anaerobic conditions can lead to the production of methane. Especially

in developed countries this can be a major source, since landfills are managed (and therefore usually covered). This causes a shift from aerobic conditions to anaerobic conditions, producing methane instead of carbon dioxide (Metz, Davidson, Bosch, Dave, and Meyer, 2007). Waste water emits methane when there is a high degradable organic content in the water, which produces methane in anaerobic conditions due to degradation (Saunois et al., 2016).

Wetlands

Following the definition from United States of Environmental Protection Agency (U.S. EPA), wetlands are ecosystems with inundated or saturated soils. Anaerobic conditions lead to methane production. The three most important factors influencing the methane production in wetlands are: temperature, anoxity and availability of substrate. After production, methane can escape from wetlands through three processes: ebullition, plant-mediated transport and molecular diffusion. Quantification of wetland methane sources is challenging due to the complicated parameterization and the definition of wetlands (Kirschke et al., 2013).

2.1.2 Sinks

The primary sinks of methane is the hydroxyl radical (OH) which accounts for approximately 90% of the methane loss (Kirschke et al., 2013). The second largest removal process of methane is soil uptake. Important about the removal by reaction with OH, is that OH is also responsible for the removal of many atmospheric gases, for example volatile organic compounds (VOC's) and carbon monoxide (CO) (Lelieveld, Gromov, Pozzer, and Taraborrelli, 2016). In case of an increase in methane concentration, which is accounted for in Representative Concentration Pathways (RCP) scenario 8.5, OH concentration will decrease and methane lifetime will increase with 8.5% from its current lifetime of 9.8 years (Voulgarakis et al., 2013).

The reaction with OH leads to a series of reactions which together form the methane oxidation chain which is displayed in Figure 2.2. In this figure it can be seen that methane reacts to formaldehyde.

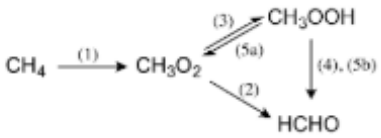

FIGURE 2.2: Methane oxidation (Source: Seinfeld and Pandis, 1998)

Formaldehyde is the first product of methane that lives longer than a few seconds. It will react according to equation 2.2 producing CO.

$$HCHO + hv + O_2 \longrightarrow 2\,HO_2 + CO \tag{2.2a}$$

$$HCHO + hv \longrightarrow H_2 + CO \tag{2.2b}$$

$$HCHO + OH + O_2 \longrightarrow HO_2 + CO + H_2O \tag{2.2c}$$

CO will than react with OH and produce carbon dioxide.

$$CO + OH + O_2 \longrightarrow CO_2 + HO_2 \tag{2.3}$$

2.2 Estimating methane emissions

Methane emissions can be estimated by two approaches.

2.2.1 Bottom-up approach

In a bottom-up approach, emissions are estimated using activity data, emission factors, and eventually country reports. These are therefore based on statistical data from all kind of sources. This methods usually gives an estimate in amount of kilogram emitted methane per year, divided in several categories. In section 3.2.3. two examples of bottom-up inventories will be presented: the TNO/MACC-III inventory and the EDGAR inventory.

2.2.2 Top-down approach

In a top-down approach, measurements of atmospheric concentrations and understanding of atmospheric processes are used to quantify emissions. The measurements can be compared to a Chemical Transport Model (CTM). A CTM converts emissions from a certain emission inventory, weather dynamics and chemistry to a methane volume mixing ratio (VMR) expressed in parts-per-billion (ppb). The simulated fields can be compared with measurements, to estimate if the implemented emissions in the model are more or less correct.

If the model simulates a certain emission peak, and this peak corresponds with measured values, the emission inventory appears to be correct. If it differs, one possible explanation is that the emissions are incorrect. For example, the emissions are to high or to low or the locations of the sources are off.

Measuring methane

Methane can be measured in situ, or indirectly with remote sensing. In situ instruments measure methane on a certain location. Remote sensing instruments, for example a satellite, has the ability to measure globally.

When studying methane abundances from sources with a model, needed are regular observations with preferably global coverage. The recently launched TROPOMI instrument will to a large extent meet these requirements. This instrument made a important step by measuring total column-mixing ratio (XCH4) not only with high resolution but also with daily global coverage. This implies that TROPOMI would be able to measure relatively small sources of methane compared to other satellites (Jacob et al., 2016).

Comparison of satellite retrievals with model output

Satellites measure XCH4 in ppb in the atmosphere. However, this measured column can not be compared directly to the total column simulation of a CTM because the satellite is sensitive with height (Rodgers and Connor, 2003).

Satellites observe sunlight reflected by earth and the atmosphere (see figure 2.3). Methane molecules in the atmosphere absorb sunlight in a certain wavelength. Therefore the light that the satellite measures in this wavelength, is dependent on the

amount of methane molecules in the atmosphere. The total methane column is estimated from the incoming light paths with a radiative transfer model, which includes path perturbations such as aerosols and cirrus.

Below a cloud the satellite has difficulty with measuring of methane, i.e. the sensitivity decreases below this cloud.

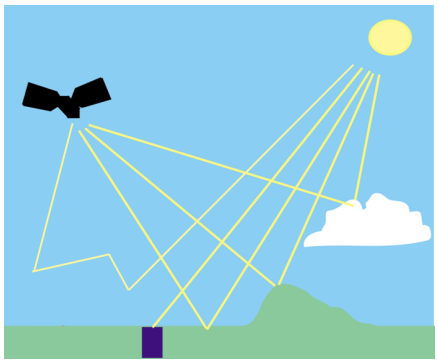

FIGURE 2.3: Light path that is measured by the satellite

Averaging kernels (AK) describe the sensitivity of the retrieved value to a prior profile. A value of one indicates that the instruments measures perfect, decreasing values mean that the instrument has difficulty with observing the trace gases at a certain height.

To make a fair comparison between the satellite and simulated profile, averaging kernels also have to applied to the model output. This method forms the basis of all comparisons between the model simulation and remote sensing instruments in this project Application of the averaging kernel is done using the following equation:

$$y = y_a + \sum_{i}^{n} AK_i * (x_i - x_{a,i}) \tag{2.4}$$

Table 2.1 gives an overview of the quantities involved when applying averaging kernels and their units. and their units. In essence, the application weights the difference between the simulated methane VMR profile and a prior methane VMR profile with the averaging kernel. The layers in the profile are then summed to obtain a column average. If the kernel values are small (low sensitivity), this main contribution will be from the the prior profile. However, if the kernel values are high, then the main contribution comes from the simulation.

Quantity	Description	Unit
y	Weighted height-averaged total column	ppb
y_a	Prior total methane column	ppb
x	Model methane profile	ppb
x_a	Prior methane profile	ppb
AK	Averaging kernels	-
i	Layer number	-
n	Number of layers	-

TABLE 2.1: Quantities used in comparison between satellite measurements and model profiles

Chapter 3

Methods

3.1 Overview

In this chapter the methods of this study will be discussed in detail. First the model set-up will be discussed. Thereafter an explanation is given of the total columns calculation and the comparison between model simulations and measurements. Additionally, the analyses of the first TROPOMI results will be explained.

3.2 Simulation model

3.2.1 Introduction to LOTOS-EUROS

LOTOS-EUROS (LE) is an open-source Eulerian CTM developed by TNO (Netherlands Organisation for applied scientific research), RIVM (National Institute for Public Health and the Environment) and KNMI (The Royal Netherlands Meteorological Institute). It is widely used as a model to calculate atmospheric concentrations. LE simulates 3D concentrations fields of trace gasses including CH_4, taking into account emissions, meteorological and chemical processes (Manders et al., 2017). In this section the model set-up will be explained as used in this project. Data used in this study is provided by TNO, unless stated otherwise.

3.2.2 Domains and resolution

In this project the methane VMR is simulated in Europe, which is the large domain. One of the goals of this project is to identify methane sources, with special interest in gas leaks from coals mines due to the connection with the Gas Leaks from Space (GALES) project (SRON, 2017). Therefore it is interesting to zoom in on Poland, since it has a large coal mining area, The Upper Silesia Coal Basin (Fix et al., 2018). This area is expected to emit large amounts of methane, which means that this source is possibly detectable with satellite measurements. The domains chosen for the simulations and the location of the Upper Silesia Basin are shown in figure 3.1.

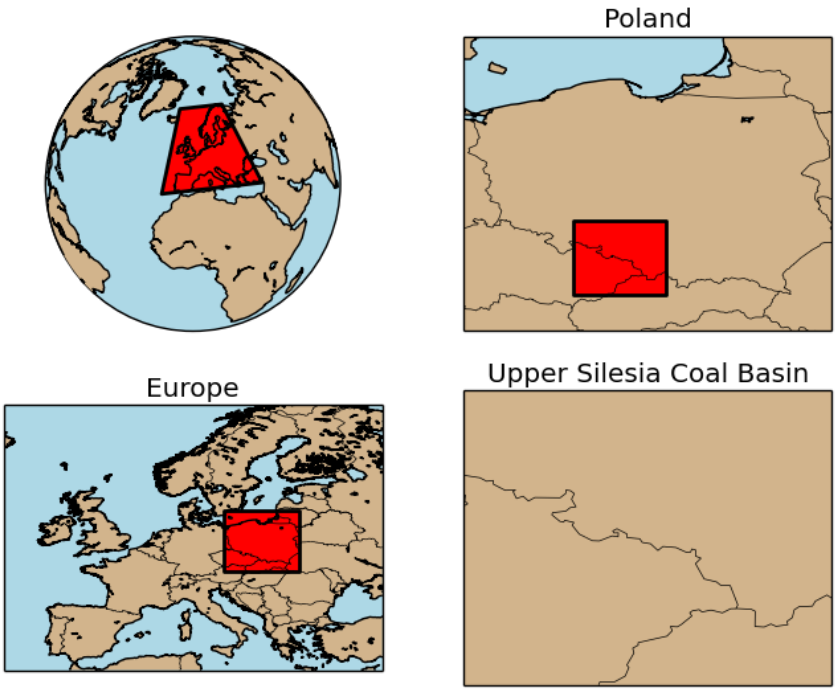

FIGURE 3.1: Domain used in this study: Europe, Poland. Location of the Upper Silesia Basin

The larger domain Europe is simulated with a resolution of 1/2 x 1/4 degrees. The zoomed-in domain Poland has a higher resolution of 1/8 x 1/16 degrees. This is needed for the comparison with TROPOMI data, which has the same resolution.

3.2.3 Emissions parameterization

In this section two inventories for anthropogenic emissions are introduced and the implementation of non-anthropogenic emissions will be discussed shortly.

Anthropogenic Emission inventories

The main emission inventory used in this project is the TNO MACC-III European anthropogenic emissions inventory. This inventory is primary based on the emissions reported by countries. The quality and consistency of reported emissions could strongly differ per country. TNO MACC-III provides an alternative inventory where the reported emissions by countries were completed with alternative emission estimates when needed. The resulting emission set covers 2003-2011 and has a high spacial resolution of 1/8 x 1/16 degrees (Kuenen, Visschedijk, Jozwicka, and Denier van der Gon, 2014).

The emission inventory is divided in different categories and sources types. The sources can be divided into point sources and area sources. Point sources are major facilities in Europe with a specific location. The remaining country total emissions over the grid were distributed as non-point sources (e.g. residential combustion, transport sectors, agriculture) with selected proxies. Table 3.1 gives an overview over the different categories used by TNO MACC-III.

Snap	Sector Name
1	Energy industries
2	Non-industrial combustion
34	Industry (combustion + processes)
5	Extraction and distribution of fossil fuels
6	Product use
7	Road transport
8	Non-road transport and other mobile sources
9	Waste treatment
10	Agriculture

TABLE 3.1: SNAP source categories used in TNO MACC-III

Another emission inventory used in this project is the the Emissions Database for Global Atmospheric Research (EDGAR). The EDGAR emission inventory is based on activity statistics and best-available emissions factors (Janssens-Maenhout et al., 2017). EDGAR is a global inventory and has a coarser resolution than TNO MACC-III.

Non-anthropogenic emissions

In the previous subsection two emission inventories were introduced which estimate the anthropogenic emissions in Europe. However, as mentioned in chapter 2, natural emissions also contribute to the total emitted amount. Therefore implementation of these emissions is also needed. For wetlands emissions the mean value of the WETcharts ensemble is used (Bloom et al., 2017. Methane flux caused by fire is provided by GFAS daily fire emissions inventory (Kaiser et al., 2012).

3.2.4 Boundary Conditions

LE simulates the atmosphere up to a certain height, varying with different versions, but never up to the top of the atmosphere. Besides, a limited horizontal domain is selected (see figure 3.1). Therefore boundary conditions are necessary the determine the inflow at the horizontal and vertical boundaries of the model, since methane is a long-lived trace gas and is transported globally.

For the boundary conditions CAMS model simulations are used. CAMS is the Copernicus Atmospheric Monitoring Service, as part from Copernicus. As mentioned in table 3.2, different CAMS products are used for 2015 and 2018. CAMS reanalysis, used for 2015, is the latest global reanalysis data set of atmospheric composition, consisting of 3D time-consistent fields for among others methane (ECMWF, 2018). Reanalysis data sets are observations reanalyzed by forecast models and data assimilation systems (Flemming et al., 2015). For the year 2018 only operational data sets are available. Operational data sets are the forecasts output by a model.

Because of the data assimilation, it is expected that the reanalysis boundary conditions will result in simulated values closer to the measured values.

3.2.5 Model simulations

In this study different models simulations have been performed with different settings. In table 3.2 an overview is given of the model simulations and the main differences. At the start of the project a test simulation of LE was performed.

Subsequently, a simulation was performed for the period July 2015 with more elaborate model settings, such as an increase in height (from 5 to 20). After discovering some flaws (see table 3.2: Timestep BC) a new simulation was performed for the whole year of 2015, with improved boundary conditions and emissions. In contrast to the simulations from 2015, a different boundary condition is used for 2018. Section 3.2.6 provides more information about these boundary conditions.

LE	Test simulation	Simulation July 2015	Simulation 2015	Simulation 2018
Layers	5	20	20	20
Resolution Europe (lon x lat)	0.5x0.25 degrees	0.5x0.25 degrees	0.5x0.25 degrees	0.5x0.25 degrees
Resolution Zoom (lon x lat)	-	0.125x0.0625 degrees	0.125x0.0625 degrees	0.125x0.0625 degrees
Vertical boundary conditions (BC)	-	CAMS73, reanalysis	CAMS73, reanalysis	CAMS C-IFS nrt
Horizontal BC Europe	-	CAMS73, reanalysis	CAMS73, reanalysis	CAMS C-IFS nrt
Horizontal BC Zoom	-	Europe simulation	Europe simulation	Europe simulation
Timestep BC	24 hours (1-day shift)	24 hours (1-day shift)	6 hours	3 hours
Layers incl. BC	5	35	35	51
Emissions	GFAS and TNO-MACC	GFAS and TNO-MACC or EDGAR	GFAS, Wetlands and TNO-MACC or EDGAR	GFAS and TNO-MACC

TABLE 3.2: Characteristics of different LE simulations

The effects on the simulated total column of some of the differences between the simulations will be discussed in chapter 4.

3.3 Study of emission inventory

In this study differences in the two used emissions inventories will be investigated. Additionally, the TNO-MACC-III inventory will be studied in more detail, given this is the default inventory for LE, and may provide more insight in what to expect from model simulations. This will be done by selecting the 10 cells with the highest emissions in Poland. The magnitude and categories of the sources in these cells will be discussed.

3.4 Total column

3.4.1 Simulation of the total column

As mentioned in Chapter 2, LE does not simulate the methane VMR to the top of the atmosphere. Since remote sensing instruments measure the total column mixing ratio, it is necessary to augment the simulated methane column with an estimate of the upper stratospheric column. Therefore output from another model is needed for the upper part of the atmosphere. The boundary conditions mentioned in the previous section are not only used as boundary conditions for LE, but also to estimate the concentration in the stratosphere. This is visualized in figure 3.2, where the vertical profile of the VMR in ppb is shown for CAMS (blue line) and LE (green line).

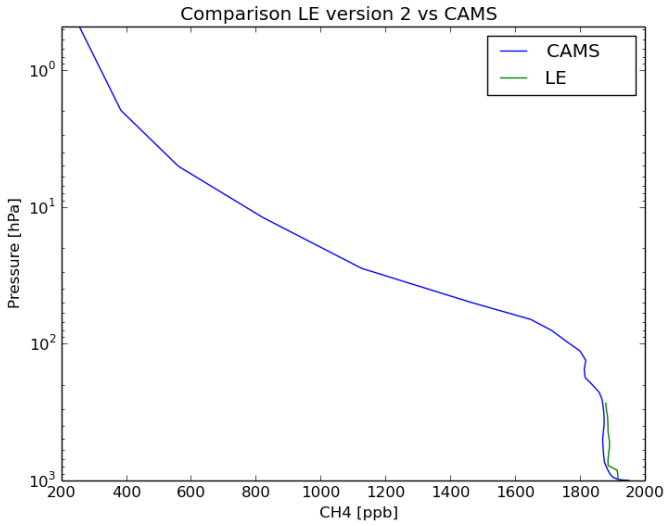

FIGURE 3.2: Example of a vertical profile LE and CAMS

LE provides the pressure levels of the borders between the layers. LE has 20 layers and therefore 21 pressure levels. The first pressure level gives the pressure at the surface. The following pressure levels give the pressure at the top of each layer. These 20 layers of LE simulate the the VMR of methane up to $\approx$ 240 hPa. From there on, simulated layers from CAMS 73 are used to augment the LE simulated layers of LE until the top of the atmosphere.

Figure 3.3 is provided to help explain this. The blocks in this figure that are number represent layers of the CAMS profile. The boundaries between the boxes represent the pressure levels. The dotted line is the top of the simulated methane profile by LE. The first CAMS 73 layer that is augmented to the LE profile is determined by pressure. For this augmentation a new layer is defined: the lower boundary is the

highest pressure level of LE, the upper boundary is a pressure level of CAMS. The latter is determined by taking the first pressure level that would physically be above LE. After this layer, the CAMS profile is augmented as is given.

The combination of LE and CAMS will from now on be called 'the model'

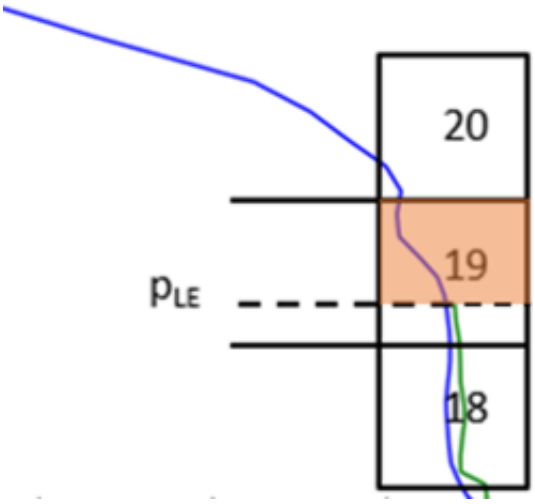

FIGURE 3.3: Schematic representation of the layers in the total column

3.4.2 Calculations

To calculate the total column mixing ratio, the amount of air molecules and methane molecules have to be calculated for each layer. This section will explain these calculations.

Some symbols will be introduced which are used to describe physical quantities. Thereafter the equations will follow.

- m = mass in kg
- M = molar mass in kg/mole
- n = amount of moles
- CH4 = methane volume mixing ratio in mole/mole
- XCH4 = total column methane volume mixing ratio in ppb
- i = layer in the model

The number of mole air in layer i can be calculated by taking the pressure difference for each layer:

$$n_{air_i} = \frac{|p_{i+1} - p_i|}{g * M_{air}} \tag{3.1}$$

LE simulates the volume mixing ratio in mole/mole in each layer ($CH4_i$). Hence the total amount of moles methane can be calculated for each layer as well:

$$n_{CH4_i} = n_{air_i} * CH4_i \tag{3.2}$$

The total column mixing ratio can be calculated by dividing the total number of methane molecules (moles) in all layers by the total number of air molecules (moles) in all layers. Multiplying this results with 10^9 results in the total column volume mixing ratio in ppb:

$$n_{air} = \sum_{i}^{35} n_{air_i} \tag{3.3}$$

$$n_{CH4} = \sum_{i}^{35} n_{CH4_i} \tag{3.4}$$

$$XCH4 = \frac{n_{CH4}}{n_{air}} * 1 * 10^9 \tag{3.5}$$

3.5 Model performance study

The study the model performance, the model simulation of the year 2015 is compared to surface observations and GOSAT and TCCON XCH4 columns.

3.5.1 Surface Observations

To verify the simulated VMR at the surface, the model result is compared to time series of surface observations stations in Europe. Observational data is gathered from the World Data Center for Greenhouse Gases (WDCGG) for the year 2015. The gathered measurements stations are Lamezia Terme (LMT), Lecce Environmental-Climate Observatory (ECO), Capo Granitola (CGR), Sonnblick (SNB), Jungfraujoch (JFJ), Plateau Rosa (PRS), Zugspitze (ZSF) and Pallas-Sammaltunturi (PAL). The locations are shown in figure 3.4. The number of locations is limited due to difficulty collecting data for 2015.

The data is sampled between 2 pm and 6 pm to avoid uncertainties in the simulated boundary layer during the night. However, some of the measurements stations are located on a mountain and need a different approach. During the day the concentration at these station can be influenced by up slope winds. However, during the night, when the boundary layer is shallow, the mountain station will usually be in the free atmosphere (Bergamaschi et al., 2005). Therefore for the mountain stations (SNB, JFJ, PRS, ZSF), only nightly values between 8 pm and 9 am are sampled. To determine which layer corresponds the best with the surface measurements on the mountain top, the correlation between the measurement stations and each layer of the model is calculated. The layer with the highest correlation is chosen to be compared with the surface measurements. Attention has been paid if the highest correlating layer is reasonable, i.e. if it is at a realistic height.

The measurements are compared to two simulations of the year 2015, one implemented with the TNO MACC-III emissions inventory and the other implemented with EDGAR emission inventory. To visualize the performance of the model outputs the observations are simply scattered against the model results. To quantify the performance of the model the correlation coefficient (r), the Root Mean Squared Error (RMSE) in ppb are calculated.

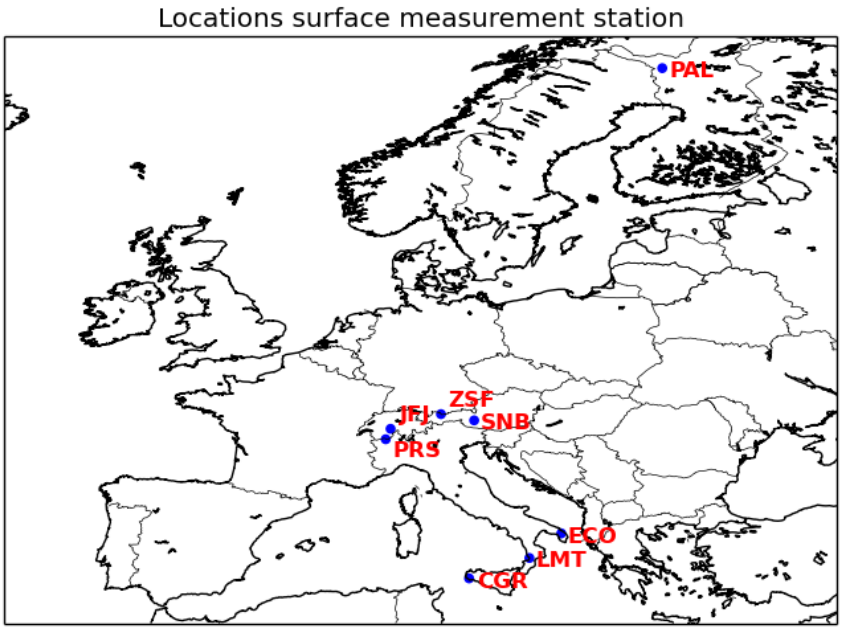

FIGURE 3.4: Locations of the used measurement stations in Europe

3.5.2 GOSAT

To validate the columns that are simulated by the model, the simulations are is compared to data from GOSAT. GOSAT is the Japanese Greenhouse gases Observing SATellite which measures among others the total column CH_4. GOSAT was launched in 2009 by the Japanese Space Agency JAXA. Radiation is observed by the Thermal And Near Infrared Sensor for Carbon Observations - Fourier Transform Spectrometer (TANSO-FTS) on board of GOSAT. GOSAT completes one orbit in about 100 minutes at a height of approximately 666 km. It takes the satellite about three days to cover the entire globe (Boesch et al., 2014).

For the comparison GOSAT level-2 observations are used: XCH4 retrieval values for each individual pixel and the corresponding prior profiles en averaging kernels(AK). These named products are defined in table 3.3 below.

Product	Description	layers	symbol
XCH4	Retrieved column-averaged dry-air mole fraction of atmospheric methane (XCH4) in nmole/mole	1	-
CH4 prior profile	A prior mole fraction profile of atmospheric CH4 in nmole/mol	4	x_a
CH4 averaging kernels	Represents the sensitivity of the retrieved XCH4 to atmospheric methane mole fraction perturbations depending on pressure (height)	4	AK
Pressure weights	Layer / level dependent weights needed to apply the averaging kernels	4	dp
Pressure levels	Layer / Vertical altitude coordinate in pressure units as used for averaging kernels	5	-

TABLE 3.3: Description GOSAT products (Boesch et al., 2014)

To make a valid comparison between GOSAT and the model, averaging kernels have to be applied, as explained in section 2.2.2. To be able to apply the averaging kernel to the simulated VMR, the simulated profile has to be remapped to 4 layers used in the retrieval product, which are defined by the pressure levels. This is done by calculating the amount of moles air and CH_2 of the model for each of the 35 layers, and assigning these to one of the 4 layers defined by the pressure levels splitting layers where necessary.

The averaging kernels are applied according to the GOSAT manual (Boesch et al., 2014):

$$y = \sum_{i}^{n}([x_{a_i} + AK_i * (x_i - x_{a_i})] * dp_i) \tag{3.6}$$

In here y is the weighted height-averaged total column which will be compared with the GOSAT XCH4 retrievals, x the interpolated simulated CH4 profiles. Other symbols are explained in table 3.3.

Every XCH4 observation from GOSAT is then compared to the corresponding y value. Comparison is made between model simulation of 2015 in the domain Europe with the corresponding GOSAT data. This is done by selecting for each pixel the the model simulation that is in the same hour. Latitude and longitude coordinates are known for the retrievals and from these coordinates the corresponding column is selected. The spatial relation is studied, by mapping the results and plotting them against the latitude and longitude. This is done for both the retrieval, the model output and the difference between them. Additionally, the spatial correlation coefficients and RMSE errors in ppb are calculated.

3.5.3 TCCON

TCCON is a network of ground-based Fourier Transform Spectrometers recording direct solar spectra in the near-infrared spectral region. From these spectra, accurate and precise column-averaged abundances of CO_2, CH_4, N_2O, HF, CO, H_2O, and HDO are retrieved (Wunch et al., 2010). The XCH4 retrievals are used to make a

comparison with the total column simulated by the model. For this comparison four stations located in Europe are used as shown in figure 3.5

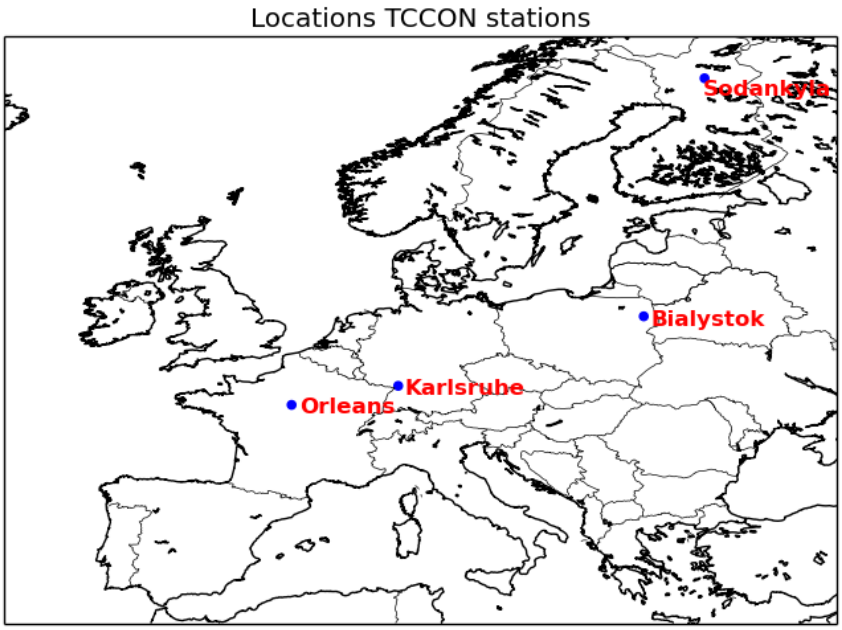

FIGURE 3.5: TCCON stations

The retrieved values are indexed by time. Data is measured approximately every few minutes. However sometimes some days are missing, mainly because of cloudiness during measurements. For the comparison of TCCON retrievals with model results again averaging kernels have to be applied, as explained in section 2.2.2.

The averaging kernels are applied according to Wunch et al., 2010. The main equation is:

$$y = y_a + h^T a^T (x - x_a) \tag{3.7}$$

Where y is the desired methane column, y_a the prior methane column both in ppb. h^T describes the vertical summation, a^T is the weighted column averaging kernel, x the methane profile simulated by the model in nmole/mole and x_a is the prior profile in nmole/mole. This equation can be rewritten as:

$$y = y_a + \frac{VC_{model} - VC_a}{VC_{air}} \tag{3.8}$$

In here VC is the Vertical Column of methane, air or prior methane in molecules/cm^2. VC_{air} is described by the following equations:

$$VC_{air} = \sum_{i}^{71} hw_i \tag{3.9}$$

$$hw_i = \frac{\Delta p_i}{g_i * m_{H2O} * (1 + f_{H2O} * \frac{m_{H2O}}{m_{air}})} \tag{3.10}$$

Where Δp_i is the difference in pressure between level i and $i+1$, g_i the gravity at level i, m_{H2O} the molar mass of air and m_{air} the molar mass of air. f_{H2O} and f_{H2O}^{dry} are the wet and dry mole fractions of water described as:

$$f_{H2O_i} = q_i * m_{air}^{dry} * m_{H2O} \tag{3.11}$$

$$f_{H2O}^{dry} = f_{H2O_i} / (1 - f_{H2O_i}) \tag{3.12}$$

VC_{model} is described as:

$$VC_{model} = \sum_{i}^{n} x_i * AK_i * hw_i \tag{3.13}$$

Where x_i is the methane profile simulated by the model and interpolated to the 71 layers defined by TCCON pressure levels and AK_i are the averaging kernels given for methane.

VC_a is described as:

$$VC_{ap} = \sum_{i}^{n} x_{a_i}^{dry} * AK_i * hw_i \tag{3.14}$$

Where $x_{a_i}^{dry}$ is the prior dry methane profile given by:

$$x_{a_i}^{dry} = x_{a_i} / (1 - f_{H2O_i}) \tag{3.15}$$

The prior methane column y_a is given by:

$$y_a = \frac{\sum_{i}^{n} x_{a_i} * hw_i}{VC_{air}} \tag{3.16}$$

The weighted height-averaged column is then compared to the TCCON retrieval. For the comparison only the column in the model is selected where the station is located in. For every TCCON measurement the corresponding simulated column and day and hour are selected. For the comparison of the model and TCCON plots are made to visualize the relationship between these two variables. Additionally, correlation coefficients, RMSE and biases for the locations are calculated.

3.6 TROPOMI

Sentinel-5 precursor is a satellite launched in October 2017 that is carrying the TROPOspheric Monitoring Instrument (TROPOMI). TROPOMI makes daily observations of trace gases, covering the entire globe and has a high resolution of 7 by 7 km.

For the comparison of model output with TROPOMI the same principles as explained in section 2.2.2 are applied. The instruction of comparison are given by (Apituley et al., 2017) and are as follows:

$$XCH4_{ref}^{avg} = VCH4_{ref}^{avg} / XAIR_{dry} \tag{3.17}$$

Where $XCH4_{ref}^{avg}$ will be compared to the s5P product after conversion to volumne mixing ratio. $XAIR_{dry}$ is the total dry air column and $VCH4_{ref}^{avg}$ is given by:

$$VCH4_{ref}^{avg} = VCH4_a + \sum_{i}^{12} AK_i * (\Delta VCH4_{ref,i} - \Delta VCH4_{a,i}) \tag{3.18}$$

Where $VCH4_a$ is the a prior total methane column in molecules/cm^2 and $\Delta VCH4_{a,i}$ the prior total methane column in molecules/cm^2 for each layer i. $\Delta VCH4_{ref,i}$ is the partial methane column in layer i in molecules/cm^2, which can be calculated with:

$$\Delta VCH4_{ref,i} = XCH4_{ref,i} * \Delta VAIR_{dry,i} \tag{3.19}$$

Where $XCH4_{ref,i}$ is the model profile converted to molecules/molecules in layer i and $\Delta VAIR_{dry,i}$ the sub dry air column in layer i in molecules/cm^2.

A brief comparison will be made between the model simulation of the year 2018 and the TROPOMI data. Since the TROPOMI data is still being processed, it is not yet corrected for aerosols and surface albedo. Therefore the relation between the retrieval and these variables will be studied.

Chapter 4

Results

In this chapter the results of this study will be presented in four section: Emission inventories, model sensitivity, model performance and TROPOMI.

4.1 Emission inventories

In this section the difference between the two emission inventories will be discussed. The TNO MACC-III inventory will also studied in depth.

4.1.1 Difference TNO MACC-III and EDGAR

Due to the different approaches between development of the emission inventories, differences between them can also be expected. Figure 4.1 shows a comparison between TNO MACC-III and EDGAR emissions for the different categories (SNAPS) in Poland. The figure shows the total methane emissions in kg/year for each category. Especially in SNAP 5 (Fossil Fuel Exploitation, see section 3.2.4.) it can be seen that the magnitude of the emission is quite different. This can possibly explained differences in emission factors (emission per activity) or by missing sources. An other possibility is that sources are covered by a different category. Other SNAPS with high emissions are Agriculture, Waste and Non-industrial combustion.

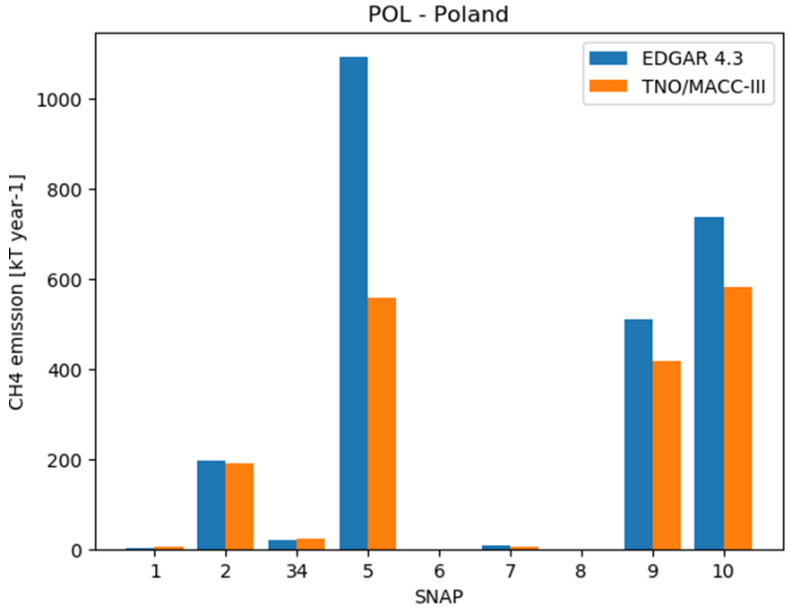

FIGURE 4.1: Difference EDGAR v2.4 and TNO MACC-III for Poland

In section 4.2.1 model results for these two implemented inventories will be discussed.

4.1.2 Emission hotspots Poland

Figure 4.2 shows the location of the 10 highest emission cells in Poland (see section 3.3). The pie charts in the top of the figure show the division among the categories for these cells. They give an impression about the categories which contribute the most to the emissions. It can be seen that agriculture, waste and fossil fuel production and distribution are dominant sources. The fossil fuel production and distribution is most dominant in the southern located group of cells (cell 0, 6, and 7). That area is a Upper Silesia Basin (see figure **??**). In cell 4 and 9 Waste is a dominant source. This could be due to a waste treatment facility in these cells. In more rural locations agriculture is a dominant source.

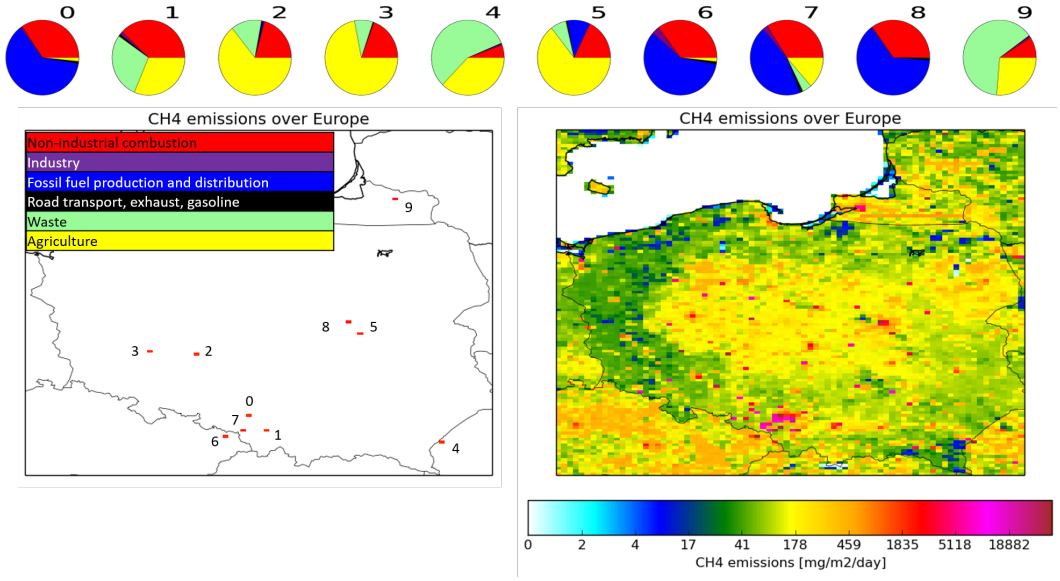

FIGURE 4.2: Division among categories for each cell

In table 4.1 more in depth information is presented about these high-emitting cells. In this table the information about the sources is split in area and point sources.

In the second column the sum of the area source emissions can be seen and in the third column the sum of point source emissions. The fourth column shows the sum of both point and area sources. Striking is that the sum of the point source emissions is in general 10 times higher as the sum of the area sources.

In the fifth and sixth column are the number of area and point sources presented. It can be seen that in general there are more area sources than point sources. However, the emitted methane is much larger for point sources than area sources.

Number	Emissions area sources (ton/year)	Emissions point sources (ton/year)	Total emission (ton/year)	Number of area sources	Number of point sources
0	2155.7	31418.1	33573.9	12	10
1	349.1	40707.1	41056.3	12	3
2	226.9	39703.2	39930.1	12	1
3	96.2	35337.6	35433.8	11	1
4	227.6	45604.5	45832.1	13	2
5	238.4	41330.5	41568.9	11	1
6	1068.8	0.	1068.8	12	2
7	341.5	65887.6	66229.2	12	6
8	2819.4	59319.3	62138.7	12	3
9	207.4	118073.4	118280.8	12	2

TABLE 4.1: CH_4 emissions from Poland

Table 4.2 presents fir each cell the most high-emitting point sources that could be found in the emission inventory. It can be seen that all sources are Landfills or Fossil fuel related activities.

Number	Emissions point source (ton/year)	Category	Source
1.	40707	5	Coal Mining
2.	39703	5	Gas Production
3.	35337	9	Landfill
4.	45359	5	Undefined
5.	41330	9	Landfill
8.	59309	9	Landfill
9.	117130	5	Oil Production

TABLE 4.2: Highest point sources

From this section it can be concluded that high emission are originated from point sources and not area sources. The highest emitters are landfills or fossil fuel related activities. Some of the highest cells are located in the Upper Silesia Basin. This confirms that this is an interesting area to study with new TROPOMI data.

4.2 Model sensitivity

In this section the results of the model sensitivity study will be discussed. The effect on model simulation of implemented emissions and different boundary conditions will be evaluated.

4.2.1 Emissions

TNO-MACC-II and EDGAR

In figure 4.3 the XCH4 averaged over 2015 are shown in Poland with on the left TNO-MACC-III and on the right EDGAR as implemented emission inventory. Int can be seen that in general the same XCH4 pattern is simulated. Differences can seen in the location and magnitude of hot spots. In figure 4.3a several hot spots in the middle of country can be seen which are not present in figure 4.3b. The simulation containing EDGAR emissions however simulates a hot spot at the coast of Poland which does not show when the TNO inventory is implemented. Both inventories identify the coal mining area in the south of Poland as a large methane source, but since the mixing ratio above the area is higher in 4.3b, it is clear that EDGAR has an higher emission estimate there. This corresponds well with the results from section 4.1.1.

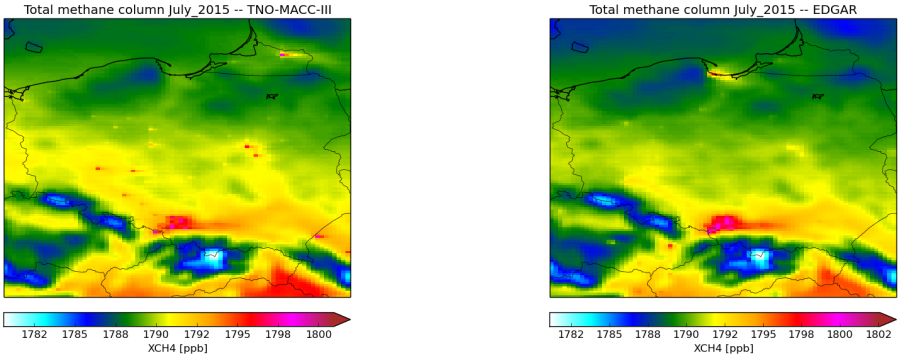

(A) Total column simulations with TNO-MACC-III emission inventory

(B) Total column simulations with EDGAR emission inventory

FIGURE 4.3: XCH4 total column mixing ratios comparison in Poland

Wetlands

Figure 4.4 shows the methane emissions of WETchart model ensemble compared to CAMS reanalysis (ra) and CAMS first guess (fg). The WETcharts shows an emission cycle with the same shape as the cycle of CAMS reanalysis. However, the peak is summer is not large enough. Still implementing the wetland emissions will improve the seasonal cycle of methane and add to the total emissions.

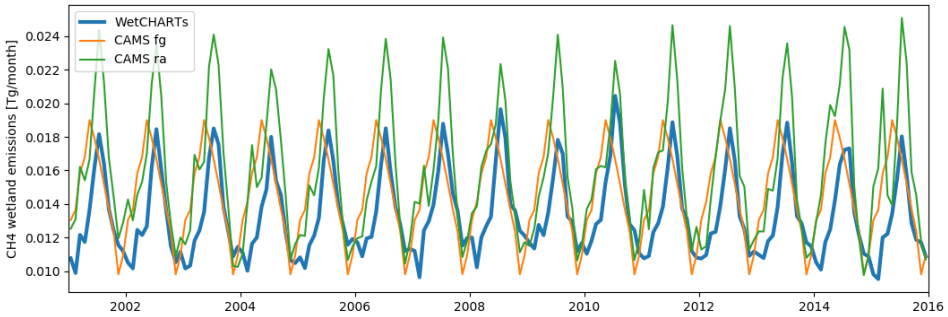

FIGURE 4.4: Wetland emissions time series for WETchart model ensemble mean, CAMS reanalysis and CAMS first guess.

Figure 4.5 shows the difference between a model simulation with wetland emissions, and a model simulation without. Clear is the increased XCH4 value in the north-east where the wetlands are located. The elevation is about 1-2 ppb in this area, which is is about 0.1%. It can be concluded that wetlands do not have a large influence. The wetlands emissions implemented come from a ensemble mean. Implementing one of these models with higher emissions resulting in a increase of 4 ppb, would still be in the TROPOMI uncertainty range. However, in other region in the world with more extensive wetlands the emissions will probably of more importance. (Hu et al., 2018). Note that in this case the influence of wetland emissions outside of Europe is included via the boundary conditions.

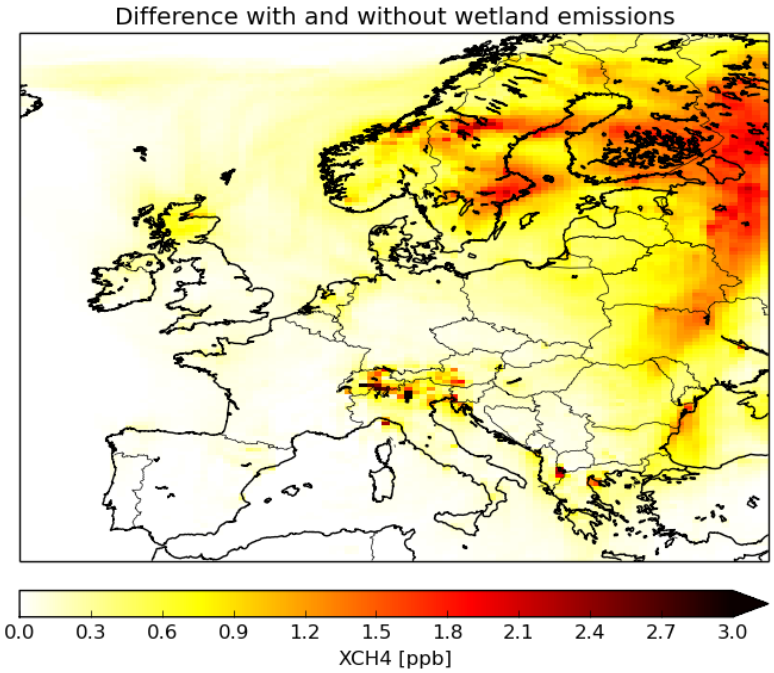

FIGURE 4.5: Difference in total column mixing ratio between simulations with and without wetland emissions.

From this section it can be concluded that the emission inventory used in the model influences only the simulated XCH4 near an identified large methane source.

For this study implementing wetland emissions is not necessary, but this may not be the case for other regions in the world with more extended wetland areas.

4.2.2 Boundary conditions

In figure 4.8a and 4.8b two simulations are shown of the averaged total column VMR over the first 10 days of July 2015. On the left a simulation with reanalysis boundary conditions and on the right the operational simulation are shown. In the left simulation, the total column mixing ratio increases to the south, but in the right simulation it increases to the north.

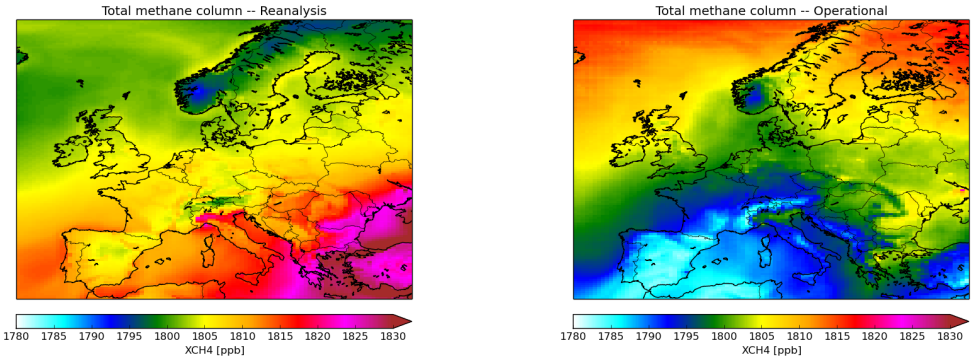

(A) Total column simulations with Reanalysis boundary conditions

(B) Total column simulations with Operational boundary conditions

FIGURE 4.6: Total column simulations with two different boundary conditions

To investigate this difference some vertical profiles are shown in figure 4.7. For both simulations a zonal averaged profiles at higher and lower latitudes are plotted. The black line represent roughly the tropopause. The blue and cyan colored line are both from the reanalysis simulation. The blue represents a zonal averaged profile at high latitudes and the cyan at low altitudes. The red and purple line represent the operational simulation. The red line represents zonal averaged profile at high latitudes and the purple at lower latitudes.

In the stratosphere it can be seen that the operational simulation profile stabilizes around a VMR of 1200 ppb. The reanalysis simulation has decreasing VMR with height. Comparing the the operational simulation profiles, it can be seen that in the lower troposphere the northern profile has higher VMR than the southern. This difference is not visible between the northern in southern profile for the reanalysis simulation.

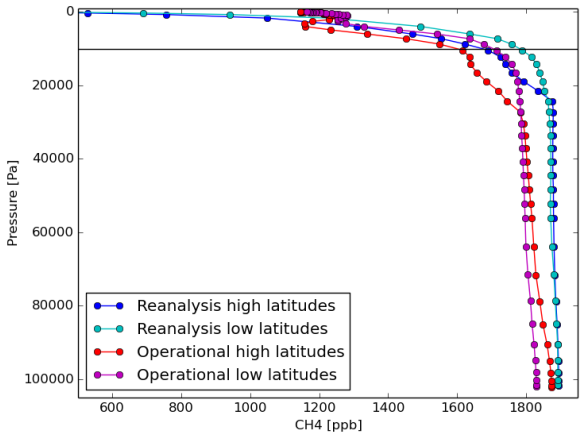

FIGURE 4.7: Vertical profiles for Operational and Reanalysis simulation. Both with a zonal averaged profile at high and low latitudes

Figure 4.8 zooms in on this difference between north and south in the troposphere. It shows a zonal averaged slice of both simulations of the troposphere. In 4.8b it can be seen that in the lower troposphere the VMR is higher in the north than in the south. This pattern is not visible in the reanalysis simulation. In the reanalysis simulation a homogeneous VMR can be seen at lower altitudes. However, the VMR is in general higher in the reanalysis simulation in the troposphere.

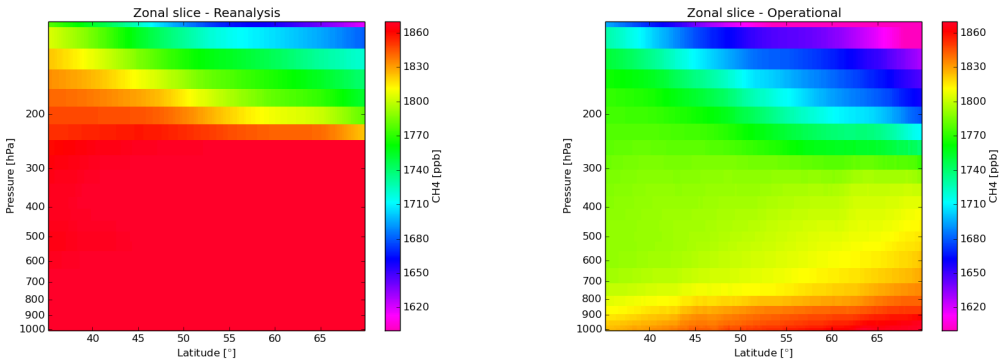

(A) Zonal averaged slice of reanalysis simulation

(B) Zonal averaged slice of operational simulation

FIGURE 4.8: Zonal averaged slice of methane simulations with different boundary conditions

It can be concluded that these different boundary conditions cause a different VMR profile. It simulates a different VMR in stratosphere, which seems to influences the VMR in the troposphere as well. This will be discussed furthermore in section 5.1.3.

Except for the comparison with TROPOMI results (year 2018), the reanalysis boundary conditions are used in this study (year 2015).

4.3 Model Performance

In this section the models ability to simulate methane VMR will evaluated. This will be done by comparing with surface observations, GOSAT and TCCON.

4.3.1 Surface observations

In this section the results of the comparison with surface observation measurements are presented. For 8 different stations a comparison is made. On overview of the locations of these measurement stations is given in chapter 3.

Figure 4.9 gives an overview of the the surface VMR in Europe averaged over the whole year 2015 for afternoon/nightly values. Most of the values of the observation locations look quite similar to the values of the surroundings, especially the locations in Italy and Finland. However, the simulations around the stations in the Alps are biased. This can be explained by the fact that these locations are in the mountains. The models has some difficulties with the orography mainly because of the large grid size. This problem may be made less significant by selecting only nighttime measurements. However, this seems not entirely solve the problem. These results therefore indicate that the dynamics in the mountain are not entirely simulated correctly yet. Incorrect emissions for mountainous areas are another possible explanation since the emissions are not zero (Kuenen et al., 2014).

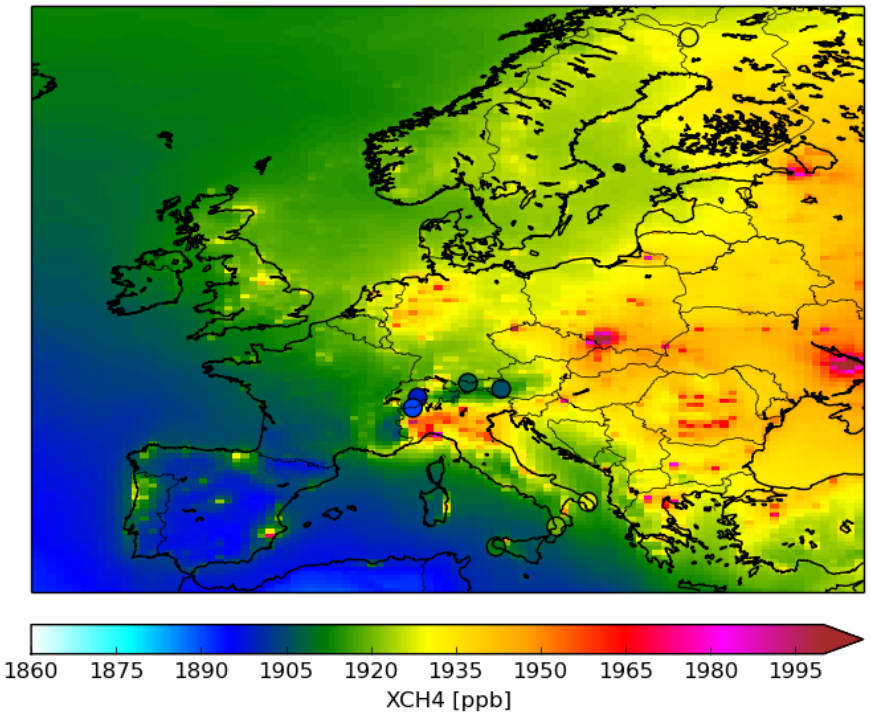

FIGURE 4.9: Time-averaged surface mixing ratios in Europe. In black circles the averaged measured mixing ratios by observation stations. Averaged time values are hourly values in the afternoon, between 4 pm and 6 pm or in the night between 8 pm and 9 am. Simulation with TNO-MACC-III emission inventory.

In figure 4.10 time series and density plots are shown for model simulations with EDGAR (middle figure) or TNO-MACC-III (right figure) emission inventory against the measurements for the three different locations. These three are chosen since the represent the type of station very well (background, mountain and normal station). The first locations that is shown in figure 4.10a is Pallas Sammaltunturi. This location seems to be simulated very well by the model with a correlation coefficient of 0.815 for both emissions inventories. There does not seems to be a large difference between the inventories. This can be explained by the fact that this station is located in the north of Finland where not many anthropogenic emissions are, and therefore the difference between TNO MACC-III and EDGAR are very small. It also indicates that the horizontal boundary conditions are rather accurate for this region.

Figure 4.10b shows the results for location Zugspitse in the Alps. The correlation coefficient is 0.652 for both inventories. However, EDGAR has a larger RMSE (22.20 ppb) than TNO-MACC-III (17.97 ppb). This means that EDGAR has more outliers than TNO-MACC-III. In the time series it can be seen that especially EDGAR simulates peaks which are not present in the measurements. This indicates that EDGAR has higher emissions near this location than TNO-MACC-III. Besides, this could mean that the measurement station is in the free atmosphere in the night, measuring a low VMR, and a simulated VMR is selected from a layer in the Planetary Boundary Layer (PBL). This results in accumulating emissions in the night, leading to higher emission peaks than the measurements for both simulations.

In figure 4.10c for location Lecce it can be seen that the opposite is happening compared to the mountain station. In the time series it can be seen that some emissions peaks measured by the station are not simulated by the model, or not in the correct magnitude. This missed peaks can also be seen in the density plot. These measurements points are visible as samples on the right-hand side of the one-to-one correspondence. The missed emission peaks can be due to any sources that are not properly implemented in the emissions inventory. Another explanation is what is called a representative error. The model simulates the methane VMR in a box of 25 by 25 km in hourly time frame. Therefore the VMR is averaged in space and time, causing peaks to be averaged out. Besides, the emission inventories usually has a flat time-profile compared to real emissions, resulting in fewer occurrence of emission peaks.

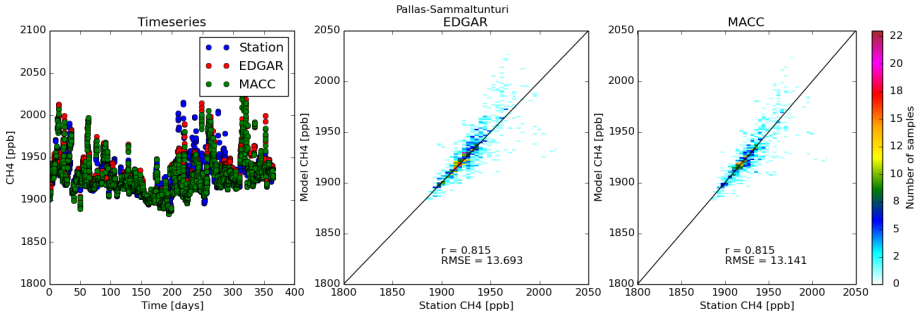

(A) Pallas Sammaltunturi

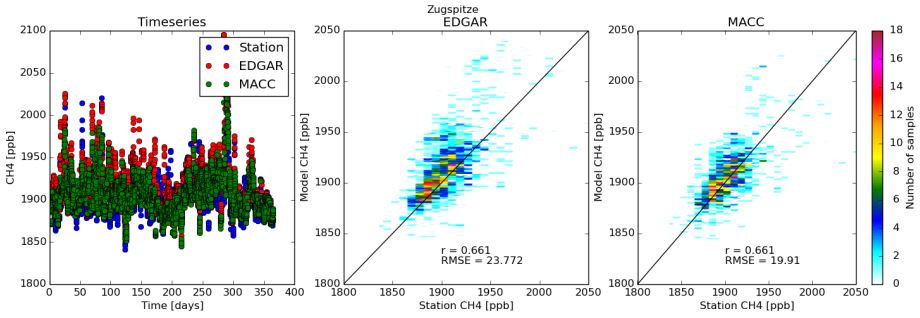

(B) Zugspitze

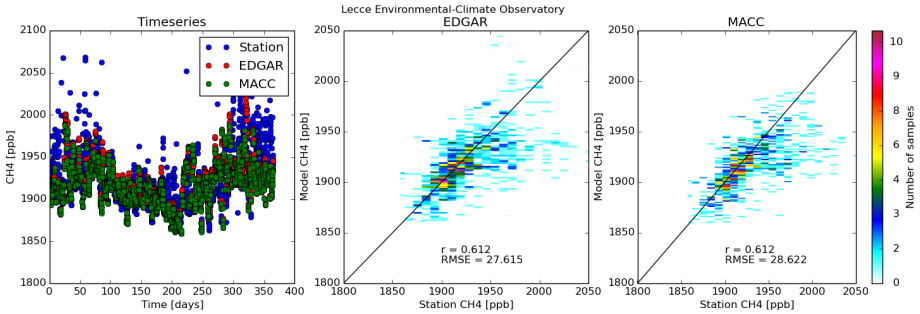

(C) Lecce Environmental-Climate Observatory

FIGURE 4.10: Comparison between the model and surface observations at multiple locations in Europe

From the surface observations it can be concluded that the model simulates the background methane VMR quite well at the surface. The simulation of methane VMR in mountainous areas and emissions peaks proves to be difficult.

4.3.2 GOSAT

In this subsection the results of the comparison of the model simulations of 2015 with GOSAT measurements will be presented. In figure 4.11 time series are plotted of the model simulation and GOSAT measurements for the domain Europe. In this figure it can be seen that both time series in general follow the same trend. However, the model has clearly as smaller spread than the GOSAT measurements. An explanation for this are the observation and retrieval errors. GOSAT has a large spread (uncertainty of 0.7%) especially compared to TCCON (uncertainty of 0.15 %) (section 4.3.3). Besides, the model spread is possibly smaller due the representation error as mentioned in the previous section.

There seems to be a general slightly lower mixing ratio in the model however. This will be studied more in the upcoming figures.

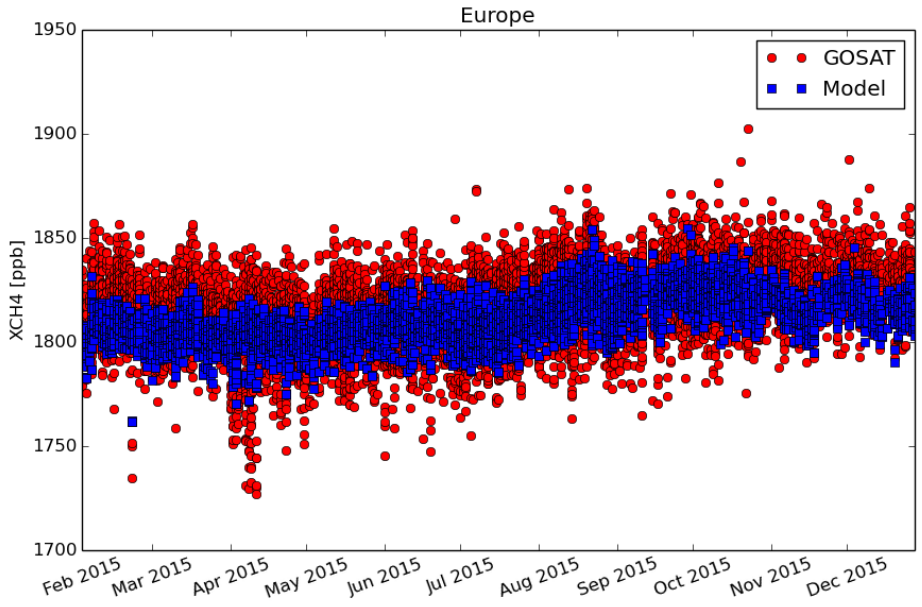

FIGURE 4.11: Time series of LE and GOSAT for the year 2015 in the domain Europe

In figure 4.12 a scatter plot is shown between the model simulation and GOSAT measurements again for 2015 in domain Europe. The color bar on the right indicates the number of data points that are in a hexagon in the figure. In general it can be seen that most data points are not far of from the model simulation since the bulk lies on the one to one correspondence. A slight tilt is however visible, indicating that higher values are more difficult to simulate correctly. In this figure it is again visible that the bulk of the data is about 5-10 ppb higher than the model simulations. A bias is found of 5.2 ppb, a RMSE of 13.6 ppb and a correlation coefficient of 0.66 for all evaluated data. This indicated that most values are not far off.

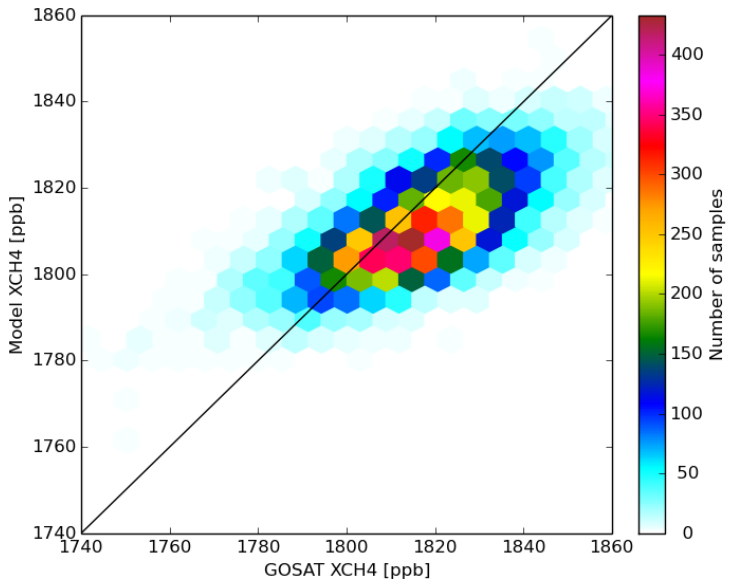

FIGURE 4.12: Scatter plot of LE and GOSAT for the year 2015 in the domain Europe

In figure 4.13 the spatial pattern of the measurements is mapped and compared to the model simulations. Figure 4.13a shows the GOSAT retrieval, figure 4.13b the model simulations and figure 4.13c the difference between the retrieval and the model simulation again for the year 2015. Striking is that the coverage is very sparse for a data set of a (almost) complete year due targeting mode. GOSAT samples three times in a very short time range (a few seconds), producing three measurements on the same location and time. Moreover data is filtered out due to obstruction of clouds. This shows that GOSAT is not very suitable for source estimation.

Looking at 4.13a, GOSAT seems to show a spatial pattern with increasing XCH4 to the south. In figure 4.13b this north to south gradient is less evident but present. It can be seen that the model overestimates the XCH4 in the north, and underestimates the XCH4 in the south. This more clearly visible in 4.13c where is visible that the model overestimates with about 10 ppb in the north and underestimates with about 15 ppb in the south.

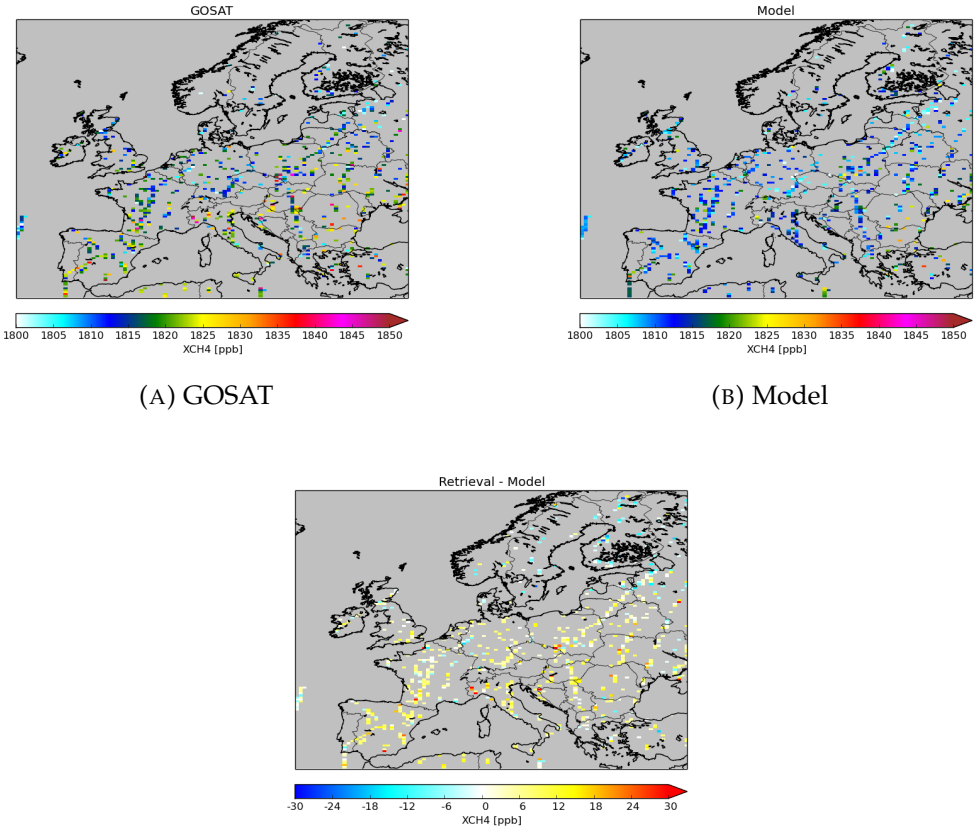

(A) GOSAT

(B) Model

(C) Difference

FIGURE 4.13: XCH4 comparison between GOSAT and the model in Europe

In figure 4.14 density plots are visible. The rows show GOSAT, the model and the difference between those, and the columns shows the latitude (left) and the longitude (right). In figure 4.14a and 4.14c the latitudinal and longitudinal gradient of the GOSAT retrieval is plotted. As was already suggested in figure 4.13a, a latitudinal gradient is visible in the GOSAT retrieval with higher values in the south and lower in the north. It should be kept in mind that satellite is always sparser in the north, as emphasized in this plot.

A longitudinal gradient could have been expected since their is a dominant west to east wind in Europe, which would blow 'clean air' to Europe, indicating that moving west emissions would get more dominant in the measured XCH4. However, this is not visible in the data. In figure 4.14c and 4.14d the latitudinal and longitudinal gradient of the model is plotted. It can be seen that the model also has an increasing XCH4 gradient towards the south as GOSAT has but it seems to be not as large. A similar longitudinal pattern is visible as for GOSAT.

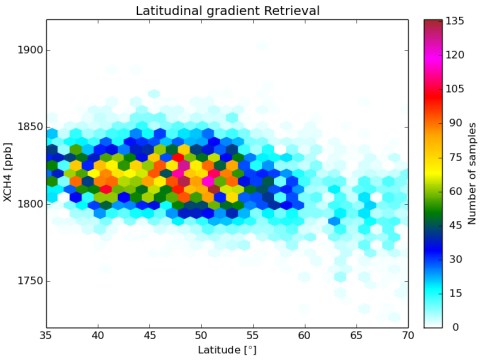

(A) GOSAT

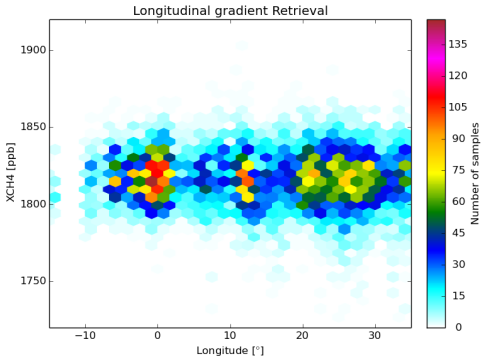

(B) Gosat

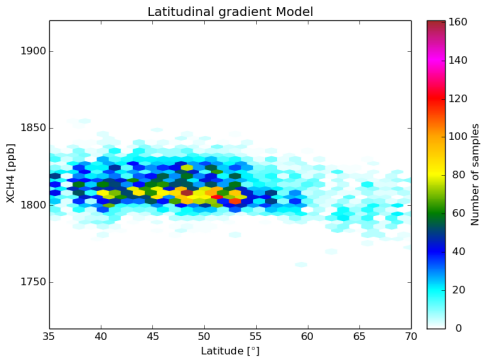

(C) Model

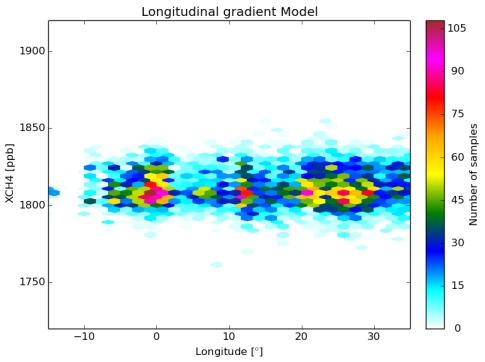

(D) Model

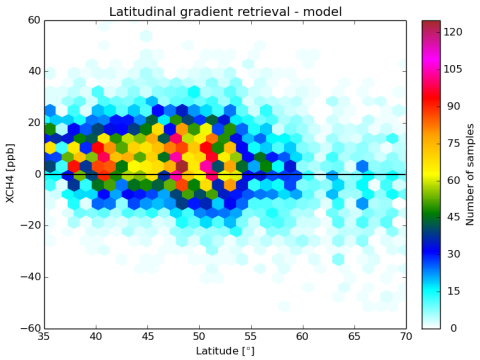

(E) GOSAT - Model

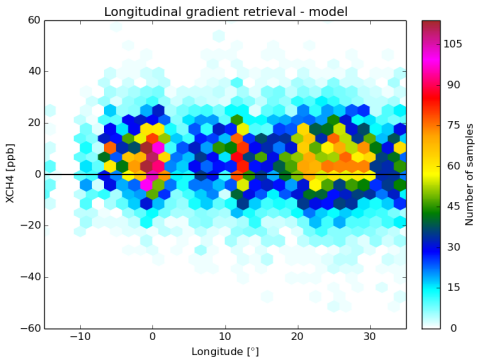

(F) GOSAT - Model

FIGURE 4.14: XCH4 against latitude (left) and longitude (right) for the year 2015 domain Europe

In general it can be concluded that the model is simulating the column averaged mixing ratio quite well, despite the underestimation of 5-10 ppb, which will be discussed in section 5.1.4.

4.3.3 TCCON

In this subsection we will be comparing simulations with XCH4 observations from the TCCON network. Figure 4.15 shows time series and scatter plots for four different locations as mentioned in Chapter 3. The locations Bialystok, Karlsruhe and Orleans seem to be simulated quite well. The time series of the model follows the trend that is also measured by the TCCON station. Even the dip in total column mixing ratio that is visible at Bialystok in the beginning of April is simulated by the model, although not as large. The dip is however rather peculiar and will therefore be investigated in detail in the next subsection. For Bialystok and correlation coefficient is found of 0.74, a RMSE of 9.5 ppb and a bias of -3.0 ppb. At Orleans is quite a large peak visible in the methane total column mixing ratio at the end of march. This is however not simulated by the model. This is probably due to an emission event not registered in the emission inventory. However it could be due to a vertical mixing error of the model. Perhaps the model mixes to fast resulting is less accumulation of mixing. For Orleans and correlation coefficient is found of 0.59, a RMSE of 9.7 ppb and a bias of -1.0 ppb.

At the stations Sodankyla the measured mixing ratio is lower than simulated. This is consistent with the measurements from GOSAT, since Sodankyla is situated in the north of Europe. GOSAT also measured lower values in the north than simulated. For further discussion about the latitudinal gradient, see section 5.1.3. For Sodankyla a correlation coefficient is found of 0.74, a RMSE of 9.5 ppb and a bias of -3.0 ppb. This is a high correlation coefficient, especially compared to the other stations, which indicates a correct trend, but just an overall higher bias.

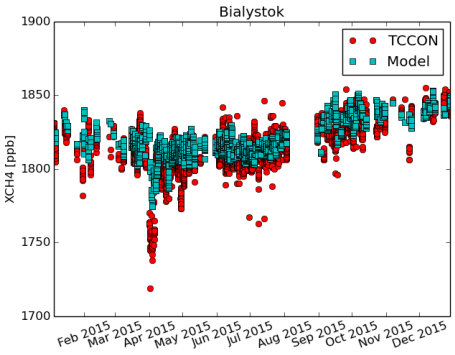

(A) Bialystok

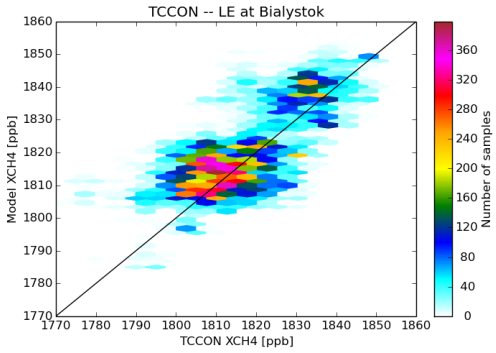

(B) Bialysto

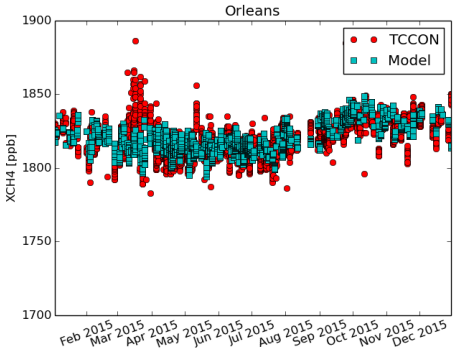

(C) Orleans

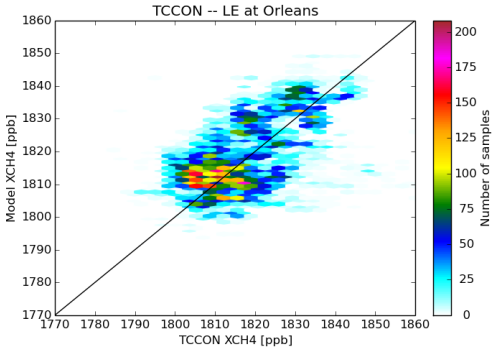

(D) Orleans

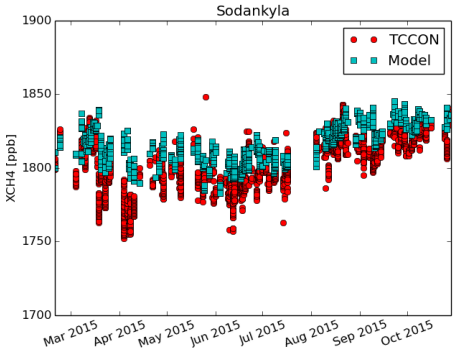

(E) Sodankyla

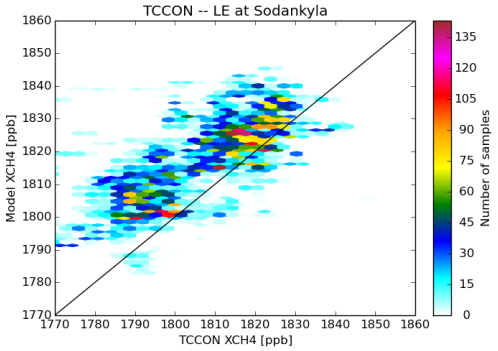

(F) Sodankyla

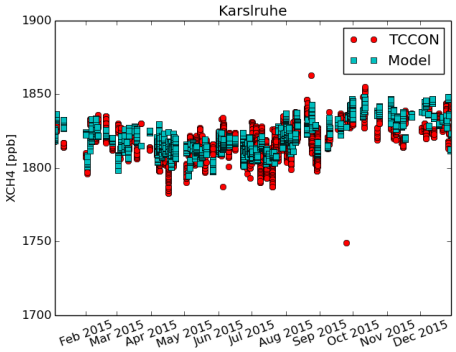

(G) Karlsruhe

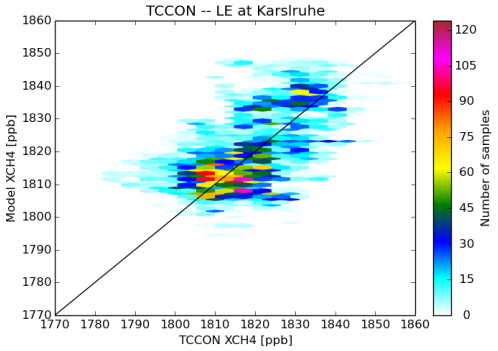

(H) Karlsruhe

FIGURE 4.15: XCH4 measurements at four different TCCON stations against XCH4 model simulations

Event April

As can be seen in figure 4.15a, there is a large depression in the total column concentration at the beginning of April. The depression is investigated to get a better understanding of the composition of the total column simulated by the model. A latitudinal slice was taken at the location from the lowest cell, which was at 23 degrees East on the fourth of April. This can be seen in figure 4.16.

In this figure it can be seen that the model also simulates a large low anomaly in the upper part of the atmosphere, simulated by the boundary conditions. As this image suggests, the anomaly comes from the the stratosphere in the north, and is probably due to the meteorological conditions spread to the south and lower heights. Because the stratosphere has a negative anomaly in the VMR, this is visible as a large anomaly model simulation and total column measurements.

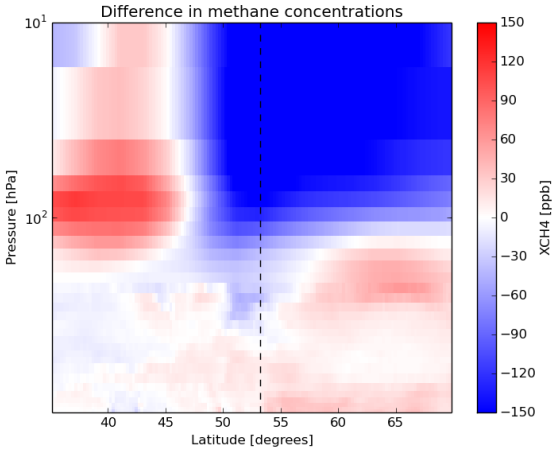

FIGURE 4.16: Latituinal slice at 23 degrees E. Difference in VMR between the fourth of April and the average of the month for each vertical layer. The dotted line shows the location of the TCCON station in Bialystok.

This analysis shows that the model is able to simulate the temporal variations measured by TCCON. However, it is not always able to simulate XCH4 peaks. Also the total column mixing ratio was overestimated by to model in the north. Further discussion about the latter is presented in section 5.1.3. A further comparison between TCCON and GOSAT is provided in section 5.1.4.

4.4 TROPOMI

4.4.1 Comparison with model simulation

In this section results of the overpasses of TROPOMI over Poland will be discussed. Due to the recent launch, low solar zenith angle in the winter and difficulties with methane retrievals, the amount of observations available was still limited for this study. However, out of the number of days that have been received, two days show good coverage of Poland.

Figure 4.17 shows the retrieval of those two days, 7th and 8th of June 2018, together with the simulation of the same days. Note that the color scales are different; this was done to be able to compare the patterns, ignoring the different absolute values

In these figures it can be seen that there is quite a difference between the simulation and the retrieval. The color bar range of simulated total column is shorter than of the retrieval. This already indicates that TROPOMI measures larger spatial differences. Furthermore, there is a difference between the mean value of both methane simulations. The retrieval has an average value of 1817 ppb and the model of 1800 ppb. However, as was visible in section 4.2.2., the boundary conditions that had to be used for the 2018 simulations caused a different VMR profile, and explains some of these differences.

Despite the different scales a careful interpretation can be made about the enhancements of the retrieval compared to the simulation. In general the model simulation is more homogeneous compared to the retrieval. The retrieval shows much more spread, even between cells near each other. In the south of Poland an enhancement is visible at the Upper Silesia Basin. The magnitude of the enhancement for simulation is >1805 ppb and for the retrieval >1840 ppb. The gradient for this enhanced area with the surrounding cells is also different. In the retrieval the difference between the enhancement at the Upper Silesia Basin its surrounding them is about 20 ppb. For the model this is about 5 ppb.

The model also simulates an enhancement over Poland going from south east to the middle of the country. This enhancement is also roughly visible in the retrieval. In the western part of Poland the retrieval sees a lower enhancement in the concentrations. This a roughly visible in the model as well.

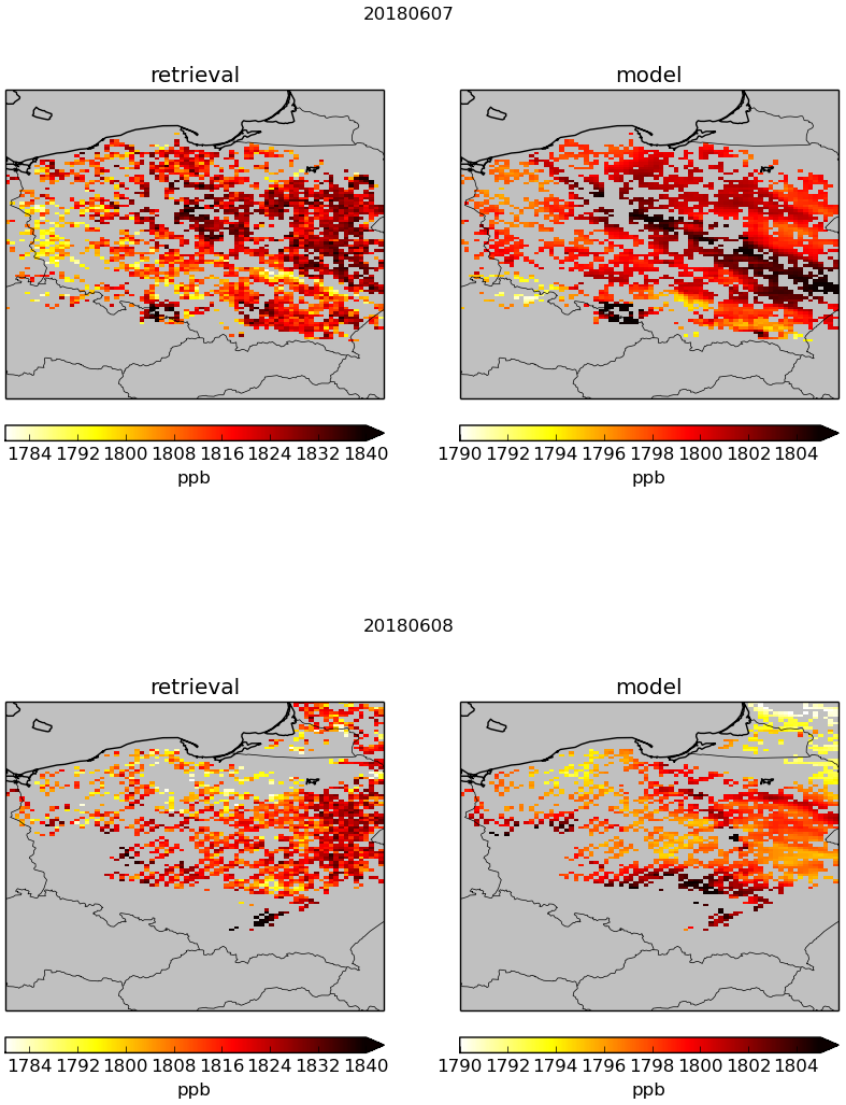

FIGURE 4.17: Comparison between XCH4 measured by TROPOMI and simulated by the model in Poland

4.4.2 Surface albedo and aersols

Due to the recent launch, TROPOMI data can be incorrect because the data is still being processed and therefore not yet corrected for aerosols and surface albedo. Therefore it is studied if there is a correlation between the signal and these variables. Figure 4.18 shows on the left side the methane retrieval of the 7th of June 2018. On the left are in the upper figure the surface albedo and in the bottom figure the aerosol column measured by TROPOMI.

In figure 4.18a a first look already suggest a relation with a high albedo leads to higher retrieval values. In the north east of Poland there is quite a large area where high surface albedo values are and also enhanced XCH4 values. There is quite a high correlation between the retrieval and the surface albedo of 0.73. However, there

should be no dependency between the amount of atmospheric methane and surface albedo.

In figure 4.18b it can clearly be seen that there is a diagonal line of enhanced values from the south east to the middle of Poland. This corresponds with the lower XCH4 values measured there. In the Upper Silesia Basin a small enhancement in aerosol column is visible, possibly influencing the retrieval. It seems there is a possible relation between the retrieval and the aerosols. There is a possibility that aerosols are emitted form the same plume as methane is. However, there is a low correlation coefficient of -0.16. From these results, the relation seems unclear.

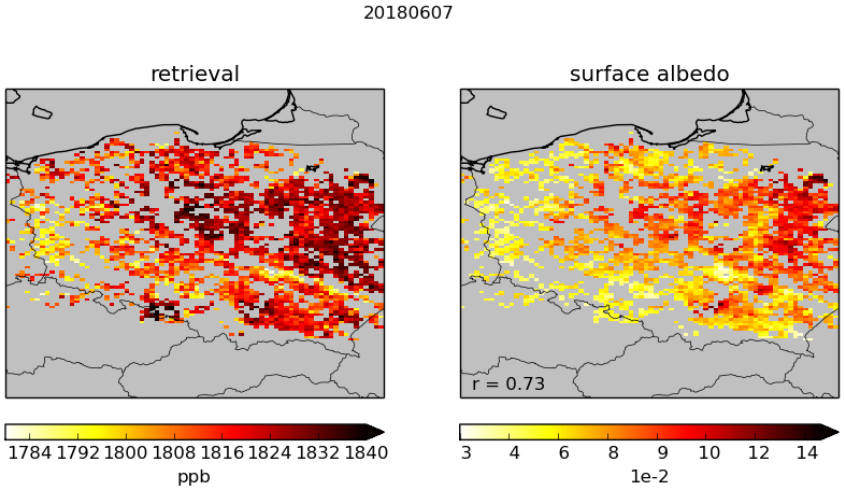

(A) XCH4 retrieval and surface albedo over Poland from TROPOMI product on 2018-06-07

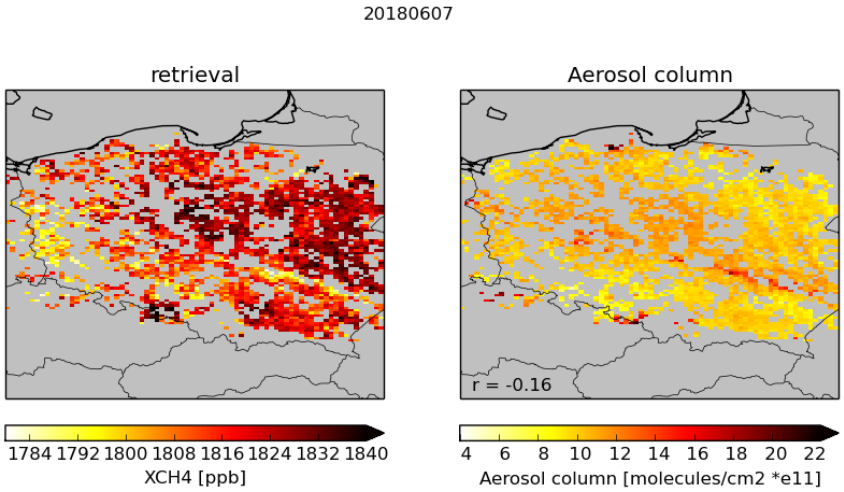

(B) XCH4 retrieval and aerosol column over Poland from TROPOMI product on 2018-06-07

FIGURE 4.18: XCH4 retrievals compared to surface albedo and aerosol columns from TROPOMI product

Previous studies show that aerosol and albedo influence the light path by scattering and absorption. However, the deviation that arises is dependent on factors such as aerosol type, size and distribution.

For example, Houweling et al., 2005 show that the combination of surface albedo and Aerosol Optical Thickness (AOT) deviate the retrieved CO_2 mixing ratio. Figure 4.19 shows the relation and balance between AOT, surface albedo and CO_2 deviations. In this figure it can be seen that lower albedo (less reflecting) causes a negative deviation in the CO_2 retrieval. A surface with a low albedo means light is absorbed by the surface, causing less light to reflect to the satellite, causing an underestimation in CO_2. However, the presence of aerosols can counteract this effect, by multiple scattering. Surfaces with a high albedo reflect sunlight back to the atmosphere, not leading to a deviation. However, combined with a high aerosol load, the aerosol cause multiple scattering, overestimating CO.

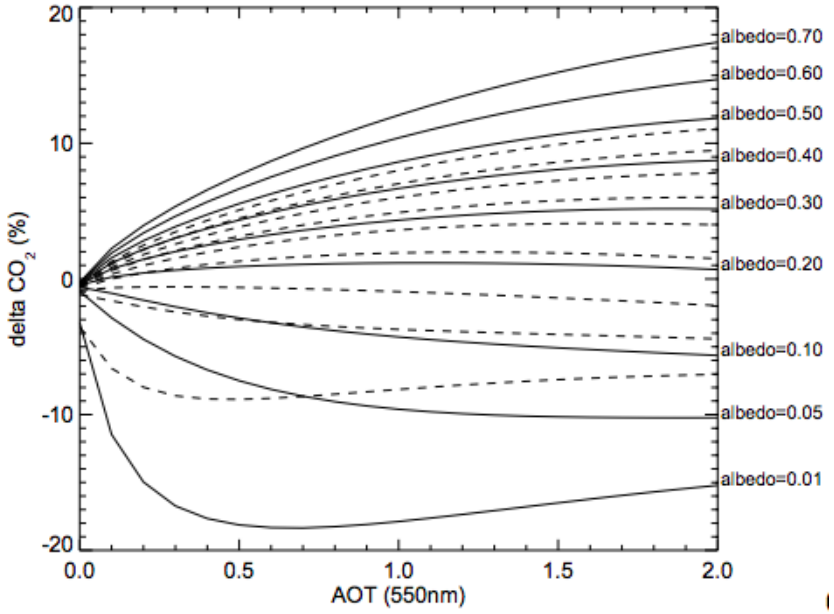

FIGURE 4.19: Relation deviation CO_s retrieval, aerosol optical thickness and surface albedo (Houweling et al., 2005)

From this section it can be concluded that TROPOMI probably sees a larger enhancement at the Upper Silesia Basin than the model does. However this can be biased by the presence of aerosols and surface albedo. Other possibilities for this difference are discussed in section 5.1.3. Besides, just one day is shown in this results, on which circumstances like a blow out, wind speed or a shallow boundary layer could influence the measured column mixing ratio. To avoid these influences, more data is needed to average over time.

Chapter 5

Discussion

In this chapter the shortcoming and improvements of this study will be discussed.

5.1 Total column calculations

When working with the simulated total column, two problems arise. The first is that for the calculation of the total column two model simulations, LE and CAMS, have to be merged. However, the top of LE is variable in height and pressure, which can lead to errors in the total columns. Second is that the simulated profile needs to be interpolated when averaging kernels are applied. This introduced a small error of about 1-3 ppb for cells in the total column, creating a error of about 0.1%. This error is however small and can be neglected on a larger scale. An error of 1-3 ppb would be an issue on a local scale. However the error is induced by pressure differences and no large pressure difference are expected between surrounding cells. Therefore it should not be a problem.

5.2 Surface observations

During this study surface observation data was gathered. Unfortunately not many stations were available for the year 2015 with a continuous measurement series. This resulted in rather few locations and not very well distributed over Europe. Four stations are clustered in the Alps and three stations are clustered in the south of Italy which limits again the knowledge that is gained from their measurements. Additionally, a location in the UK or Ireland would be preferred since it would give us information about the influence of the horizontal boundary conditions and if these are correct. This is because wind from west to east is dominant in Europe which means air from the boundary conditions is mainly blown into the domain from the west. A station at the western boundary would therefore provide this information. For future studies it would be recommended to include more stations, especially at the western boundary, when observational data for 2015 is available. Another possibility is to repeat this study for a year before 2015, for which sufficient data is available.

5.3 Model boundary conditions

From the comparisons between simulations and GOSAT and/or TCCON XCH4 columns there was one clear aspect of the model simulation that was incorrect: the latitudinal gradient. Both measured a lower total column mixing ratio in the north of Europe. No TCCON station is present in the south, but GOSAT did measure a

higher total column mixing ratio in the south than the model simulated. This indicates that the model simulates a different total column mixing ratio gradient than is measured. However, the surface VMR in north of Europe was very similar to the measured VMR. This indicates that this incorrect gradient is due to stratospheric mixing ratios, which is very plausible explanation since it is difficult to verify stratospheric VMR. Satellites measure only the total column and not that many aircraft measurements are done in the stratosphere.

From the total column simulations it is clear that the boundary conditions contribute to the total column VMR. However, an incorrect gradient would perhaps not prove to be a big issue for source estimation, because source estimation focuses on the VMR at the source in comparison to its surroundings. An incorrect stratospheric gradient would not influence this comparison on the small scale of a source.

However, we have seen that strongly biased boundary conditions, such as the simulated conditions for 2018 are troublesome. As shown in figure 4.7, these boundary conditions contained VMR values of 1200 ppb at the top of the stratosphere which is much higher than present in the boundary conditions used for 2015. It seems that these incorrect stratospheric VMR influence the tropospheric VMR. An VMR enhancement was found in the north of Europe. A possible explanation for this is that the high VMR from the stratosphere in the north is transported to the troposphere in the north. This happens due to global circulation of air, where air is transported to the stratosphere at the tropics and back to the troposphere at the poles. Since the VMR in the troposphere is usually low as in the simulation of 2015, no high VMR arises at the surface in the north for this simulation.

5.4 Simulation of spatial gradient

At first sight, the spatial gradients in the TROPOMI data are much stronger than the gradients simulated by the model. Since there was only one day of data, this finding is not conclusive yet, but certainly interesting for further research. Due to the spatial sparse data from TCCON and GOSAT this has not been noticed before. Different processes can be the cause of this. Perhaps the emissions implemented in the model are too low. Another possible explanation is the incorrect vertical mixing of the model. If this vertical mixing is too strong, no accumulation of methane takes place at the source and a lower VMR will be simulated. It can also partly be explained by a representation error. Besides, it should not be forgotten however that TROPOMI possibly also measures an incorrect enhancement due to the influence of aerosols and surface albedo.

5.5 Satellite height sensitivity

Remote sensing instruments have a different sensitivity with height. Where they are not very sensitive, the profile will look more like the prior profile. GOSAT and TCCON measurements seem to differ from each other in this study. However the model simulations smoothend by the kernels of both remote sensing instruments can not be compared due to different averaging kernels and prior profiles. Where GOSAT is most sensitive at higher altitudes, TCCON is most sensitive at the surface.

Chapter 6

Conclusion

The aim of this study was to work towards estimating methane sources with TROPOMI and LOTOS-EUROS. To reach this aim, four sub-questions were defined which will be answered in this chapter. Additionally a outlook and an overall final word will be given.

6.1 What are the known sources for methane and how are they quantified in inventories?

In this project, two emission inventories were studied: TNO-MACC-II and EDGAR. They divide emissions in different categories with point and area sources. For Poland the two inventories showed a large difference in estimated emission from fossil fuel exploitation and extraction, one of the largest sources. Other large sources were agriculture and waste. TNO-MACC-III emission inventory showed that point sources are dominant over area sources. Specific large methane sources are coal mines and landfills.

6.2 How sensitive is the model for different emission input and boundary conditions?

To answer this question, the sensitivity of the model on three different aspects were studied: anthropogenic emissions, wetlands emissions en boundary conditions. From these results it can be concluded that especially the boundary conditions have a large influence in the overall methane total column mixing ratio. Inaccurate boundary conditions can cause an incorrectly simulated stratospheric gradient, influencing the total column mixing ratio.

Anthropogenic emissions mainly influence the total column mixing ratio where large methane point sources are located. The influence of wetlands seems to be rather small in Europe, but could be more important in other parts of the world with extended wetland areas.

6.3 How does the model perform compared to methane observations?

The model has been validated with different type of measurements: continuous surface observation, GOSAT and TCCON total columns. After several modifications the model seems to perform quite well, with in general methane VMR of the appropriate order. This was not known before the start of this project and therefore already

a fine accomplishment. The simulation of the VMR in the troposphere seems quite good based on the comparison with surface observations.

From the compassion with GOSAT and TCCON total column it can be concluded that the total column mixing ratio's are as well simulated in the right order of magnitude. On a large scale it is visible that the model simulates an incorrect gradient form north to south in XCH4. This is probably induced by an incorrect VMR gradient in the boundary conditions.

On a smaller scale, the comparison with TROPOMI suggest that the model simulation of spatial XCH4 gradients are too flat. This is probably partly caused by a flat emission inventory and the use of spatial and temporal averages for representation of observations. However, imperfect mixing in the model is also a possible cause of uncertainty and needs further research.

6.4 What emission sources are visible in the first TROPOMI data?

From the first TROPOMI results it can be concluded that the Upper Silesia Coal Basin is probably a large sources of methane although the strength is still uncertain. One reason for this uncertainty is that the data is sparse, and the high concentration can be caused by other factors such as meteorological conditions. Besides, the data was not yet corrected for surface albedo and aerosol. The results however suggest that TROPOMI will be able to quantify sources of this magnitude in the future. More data is needed to conclude on Upper Silesia Basin, but also on other possible sources in Poland. This way TROPOMI can maybe help in conclude on the locations of the sources and the magnitude.

6.5 Outlook

As happens with most studies, goals change during the scope of the project. Starting this project it was planned to study TROPOMI data in two different study areas. However due to circumstances the TROPOMI data was provided later than expected. Therefore an extensive analyses has not been done yet and probably will be done in the future, since this study has already shown some interesting results with relatively little data. The results in this study are promising for the future when enough data is available for a full analysis. Possible is that with enough data and enough coverage, methane sources really can be identified and quantified, which would hopefully provide valuable information to improve emission inventories and help reduce methane emissions. A repetition of this study would be recommended when more ground based en TROPOMI data is available.

6.6 Final word

Overall it can be concluded that LE has the potential to become a well performing model in simulating methane concentration. Together with newly developed high quality satellites such as TROPOMI, it could absolutely improve our knowledge of methane sources on our planet, and hopefully help reducing global warming.

Bibliography

Apituley, A., Pedergnana, M., Sneep, M., Veefkind, J. P., Loyola, D., & Hasekamp, O. (2017). Sentinel-5 precursor/tropomi level 2 product user manual methane. Accessed on 07.06.2018. Retrieved from https://sentinels.copernicus.eu/documents/247904/2474726/Sentinel-5P-Level-2-Product-User-Manual-Methane

Bergamaschi, P., Krol, M., Dentener, F., Vermeulen, A., Meinhardt, F., Graul, R., ... Dlugokencky, E. (2005). Inverse modelling of national and european ch 4 emissions using the atmospheric zoom model tm5. *Atmospheric Chemistry and Physics*, *5*(9), 2460.

Blake, D. R., Mayer, E. W., Tyler, S. C., Makide, Y., Montague, D. C., & Rowland, F. (1982). Global increase in atmospheric methane concentrations between 1978 and 1980. *Geophysical Research Letters*, *9*(4), 477–480.

Bloom, A. A., Bowman, K. W., Lee, M., Turner, A. J., Schroeder, R., Worden, J. R., ... Jacob, D. J. (2017). A global wetland methane emissions and uncertainty dataset for atmospheric chemical transport models (wetcharts version 1.0). *Geoscientific Model Development*, *10*(6), 2141–2156. doi:10.5194/gmd-10-2141-2017

Boesch, H., Buchwitz, M., Chevallier, F., Detmers, R., Dils, B., Frankenberg, C., ... C.Frankenberg. (2014). Product specification document version 3 (psdv3). Accessed on 20.03.2018. Retrieved from http://www.esa-ghg-cci.org/index.php?q=webfm_send/160

Ciais, P. [P.], Sabine, C., Bala, G., Bopp, L., Brovkin, V., Canadell, J., ... Thornton, P. (2013). Carbon and other biogeochemical cycles. In T. Stocker, D. Qin, G.-K. Plattner, M. Tignor, S. Allen, J. Boschung, ...P. Midgley (Eds.), *Climate change 2013: The physical science basis. contribution of working group i to the fifth assessment report of the intergovernmental panel on climate change* (Chap. 6, pp. 465–570). Cambridge, United Kingdom: Cambridge University Press. doi:10.1017/CBO9781107415324.015

ECMWF. (2018). Cams reanalysis data documentation. Accessed on 26.07.2018. Retrieved from https://confluence.ecmwf.int/display/CKB/CAMS+Reanalysis+data+documentation

EIA. (2017). Natural gas explained. Accessed on 23.05.2018. Retrieved from https://www.eia.gov/energyexplained/index.php?page=natural_gas_homes

Fix, A., Amediek, A., Bovensmann, H., Ehret, G., Gerbig, C., Gerilowski, K., ... Zöger, M. (2018). Comet: An airborne mission to simultaneously measure co2 and ch4 using lidar, passive remote sensing, and in-situ techniques. In *Epj web of conferences* (Vol. 176, p. 02003). EDP Sciences.

Flemming, J., Huijnen, V., Arteta, J., Bechtold, P., Beljaars, A., Blechschmidt, A.-M., ... Tsikerdekis, A. (2015). Tropospheric chemistry in the integrated forecasting system of ecmwf. *Geoscientific Model Development*, *8*(4), 975–1003. doi:10.5194/gmd-8-975-2015

Houweling, S., Hartmann, W., Aben, I., Schrijver, H., Skidmore, J., Roelofs, G.-J., & Breon, F.-M. (2005). Evidence of systematic errors in sciamachy-observed co 2 due to aerosols. *Atmospheric Chemistry and Physics*, *5*(11), 3003–3013.

Hu, H., Landgraf, J., Detmers, R., Borsdorff, T., Aan de Brugh, J., Aben, I., ... Hasekamp, O. (2018). Toward global mapping of methane with tropomi: First results and intersatellite comparison to gosat. *Geophysical Research Letters*, *45*(8), 3682–3689.

Jacob, D. J., Turner, A. J., Maasakkers, J. D., Sheng, J., Sun, K., Liu, X., ... Frankenberg, C. (2016). Satellite observations of atmospheric methane and their value for quantifying methane emissions. *Atmospheric Chemistry and Physics*, *16*(22), 14371–14396.

Janssens-Maenhout, G., Crippa, M., Guizzardi, D., Muntean, M., Schaaf, E., Dentener, F., ... Peters, J., et al. (2017). Edgar v4. 3.2 global atlas of the three major greenhouse gas emissions for the period 1970–2012. *Earth Syst. Sci. Data Discuss*.

Kaiser, J., Heil, A., Andreae, M., Benedetti, A., Chubarova, N., Jones, L., ... Suttie, M., et al. (2012). Biomass burning emissions estimated with a global fire assimilation system based on observed fire radiative power.

Kirschke, S., Bousquet, P., Ciais, P. [Philippe], Saunois, M., Canadell, J. G., Dlugokencky, E. J., ... Bruhwiler, L., et al. (2013). Three decades of global methane sources and sinks. *Nature geoscience*, *6*(10), 813.

Kuenen, J. J. P., Visschedijk, A. J. H., Jozwicka, M., & Denier van der Gon, H. A. C. (2014). TNO-MACC_II emission inventory; a multi-year (2003-2009) consistent high-resolution european emission inventory for air quality modelling. *Atmospheric Chemistry and Physics*, *14*(20), 10963–10976. doi:10.5194/acp-14-10963-2014

Lelieveld, J., Gromov, S., Pozzer, A., & Taraborrelli, D. (2016). Global tropospheric hydroxyl distribution, budget and reactivity. *Atmospheric Chemistry and Physics*, *16*(19), 12477.

Manders, A. M., Builtjes, P. J., Curier, L., van der Gon, D., Hugo, A., Hendriks, C., ... Segers, A. J., et al. (2017). Curriculum vitae of the lotos–euros (v2. 0) chemistry transport model. *Geosci Model Dev 2017; 10: 4145-73*.

Metz, B., Davidson, O. R., Bosch, P. R., Dave, R., & Meyer, L. A. (2007). Contribution of working group iii to the fourth assessment report of the intergovernmental panel on climate change, 2007. Cambridge University Press, Cambridge, UK.

Myhre, G., Shindell, D., Bréon, F.-M., Collins, W., Fuglestvedt, J., Huang, J., ... Zhang, H. (2013). Anthropogenic and natural radiative forcing. In T. Stocker, D. Qin, G.-K. Plattner, M. Tignor, S. Allen, J. Boschung, ...P. Midgley (Eds.), *Climate change 2013: The physical science basis. contribution of working group i to the fifth assessment report of the intergovernmental panel on climate change* (Chap. 8, pp. 659–740). Cambridge, United Kingdom: Cambridge University Press. doi:10.1017/CBO9781107415324.018

Neef, L., van Weele, M., & van Velthoven, P. (2010). Optimal estimation of the present-day global methane budget. *Global biogeochemical cycles*, *24*(4).

Rodgers, C. D. & Connor, B. J. (2003). Intercomparison of remote sounding instruments. *Journal of Geophysical Research: Atmospheres*, *108*(D3).

Saunois, M., Bousquet, P., Poulter, B., Peregon, A., Ciais, P., Canadell, J. G., ... Zhu, Q. (2016). The global methane budget 2000-2012. *Earth System Science Data*, *8*(2), 697.

Seinfeld, J. H. & Pandis, S. N. (1998). *Atmospheric chemistry and physics: From air pollution to climate change*. John Wiley & Sons.

SRON. (2017). Tropomi will detect methane leakages from space. Accessed on 24.01.2018. Retrieved from https://www.sron.nl/news/4714-tropomi-gaat-methaanlekken-opsporen-vanuit-de-ruimte

Voulgarakis, A., Naik, V., Lamarque, J.-F., Shindell, D. T., Young, P., Prather, M. J., ... Cameron-Smith, P., et al. (2013). Analysis of present day and future oh and methane lifetime in the accmip simulations. *Atmospheric Chemistry and Physics*, *13*(5), 2563–2587.

Wunch, D., Toon, G. C., Wennberg, P. O., Wofsy, S. C., Stephens, B. B., Fischer, M. L., ... Biraud, S. C., et al. (2010). Calibration of the total carbon column observing network using aircraft profile data.